Summertime productivity and carbon export potential in the Weddell Sea, with a focus on the waters adjacent to Larsen C Ice Shelf

Raquel F. Flynn[1*], Thomas G. Bornman[2,3], Jessica M. Burger[1], Shantelle Smith[1], Kurt A.M. Spence[1] and Sarah E. Fawcett[1,4]

[1]Department of Oceanography, University of Cape Town, Cape Town, South Africa

[2]South African Environmental Observation Network, Elwandle Coastal Node, Port Elizabeth, South Africa

[3]Institute for Coastal and Marine Research, Nelson Mandela University, Port Elizabeth, South Africa

[4]Marine and Antarctic Research centre for Innovation and Sustainability (MARIS), University of Cape Town, Cape Town, South Africa

[*]*Correspondence to*: Raquel F. Flynn (flyraq001@myuct.ac.za)

Abstract

The Weddell Sea (WS) represents a point of origin in the Southern Ocean where globally-important water masses form. Biological activities in WS surface waters thus affect large-scale ocean biogeochemistry. During summer 2018/2019, we measured net primary production (NPP), nitrogen (nitrate, ammonium, urea) uptake, and nitrification in the western WS at the Antarctic Peninsula (AP) and Larsen C Ice Shelf (LCIS), in the southwestern Weddell Gyre (WG), and at Fimbul Ice Shelf (FIS) in the south-eastern WS. The highest average rates of NPP and greatest nutrient drawdown occurred at LCIS. Here, the phytoplankton community was dominated by colonial *Phaeocystis antarctica*, with diatoms increasing in abundance later in the season as sea-ice melt increased. At the other stations, NPP was variable, and diatoms known to enhance carbon export (e.g., *Thalassiosira* spp.) were dominant. Euphotic zone nitrification was always below detection, such that nitrate uptake could be used as a proxy for carbon export potential, which was highest in absolute terms at LCIS and the AP. Surprisingly, the highest f-ratios occurred near FIS rather than LCIS (average of 0.73 ± 0.09 versus 0.47 ± 0.08). We attribute this to partial ammonium inhibition of nitrate uptake at LCIS (where ammonium concentrations were 0.6 ± 0.4 μM, versus 0.05 ± 0.1 μM at FIS) driven by increased heterotrophy following the accumulation of nitrate-fuelled phytoplankton biomass in early summer. Across the WS, carbon export appears to be driven by a combination of physical, chemical, and biological factors, with the highest export flux occurring at the ice shelves and lowest in the central WG.

Keywords: Nitrogen uptake, primary production, phytoplankton taxonomy, nutrient depletion, ammonium inhibition, Antarctic ice shelves

1. Introduction

The Southern Ocean is an important driver of Earth's climate as it transports large quantities of heat and dissolved gases, and supplies 65-85% of the global ocean's nutrients (Keffer and Holloway 1988; Sarmiento et al. 2004; Frölicher et al. 2015; Keller et al. 2016). Despite the Southern Ocean's central role in atmospheric CO_2 removal (DeVries 2014; Frölicher et al. 2015; Gruber et al. 2019), the incomplete drawdown of nutrients (i.e., nitrate, phosphate, and silicic acid) in its surface waters due to iron and light limitation of phytoplankton (Martin et al. 1991; Sunda and Huntsman 1997) represents a missed opportunity for CO_2 removal (Sarmiento and Toggweiler 1984). The Weddell Sea constitutes a point of origin in the Southern Ocean where water masses form and communicate with the atmosphere before subducting (Muench and Gordon 1995; Talley et al. 2011), thereby setting the initial physical and chemical conditions of the deep global ocean. Biogeochemical cycling in the surface Weddell Sea thus has implications for carbon transfer to and storage within the ocean interior (Hoppema et al. 2004; Kerr et al. 2018). The southern and western Weddell Sea are bounded by ice shelves, which promote high rates of summertime productivity, nutrient drawdown and carbon export (El-Sayed and Taguchi 1981; Hoppema and Goeyens 1999; Hoppema et al. 2000) largely because the surface ecosystem is less iron- and light-limited in the ice shelf-adjacent waters than in open waters (Klunder et al. 2014).

The Weddell Sea is separated from the Antarctic Circumpolar Current (ACC) and open Southern Ocean by the Weddell Sea fronts (Orsi et al. 1995). The general large-scale circulation takes the form of a cyclonic, wind-driven and topographically-steered gyre, the Weddell Gyre (WG) (Fahrbach et al. 1994, 1995; Orsi et al.1995), that transports the relatively warm, saline waters of the ACC into the polar region where they are cooled and become more saline (Huhn et al. 2008; Nicholls et al. 2009; van Caspel et al. 2015). The production of dense bottom water is thought to occur at two sites in the Weddell Sea: at Filchner-Ronne Ice Shelf (FRIS) and Larsen C Ice Shelf (LCIS) (Gordon et al. 1993; Schröder et al. 2002; Schodlok et al. 2002). Here, Modified Warm Deep Water (MWDW) intrudes onto the continental shelf and mixes with Antarctic Surface Water (ASW). ASW is cooled to freezing point through heat loss to the atmosphere, as well as being supercooled under the ice shelves, and increases in salinity due to brine rejection during sea-ice formation, which further increases its density (Brennecke 1921; Mosby 1934; Gill 1973). As MWDW flows throughout the WG, its physical and chemical properties are altered due to mixing with ASW, ultimately resulting in the formation of dense bottom waters. Upon reaching the Antarctic Peninsula (AP), the transformed bottom waters either spill out over the shelf and re-enter the ACC or are entrained into the eastward flowing limb of the WG (Orsi et al. 1993; Locarnini et al. 1993).

Weddell Sea surface waters are warm and saline while those over the continental shelf are relatively cool and fresh (Nicholls et al. 2004). These different waters are separated by the Antarctic Slope Front (ASF; Jacobs 1986; 1991), a fast-flowing jet situated between the 500 m and 1000 m isobath that separates the Open Ocean Zone (OOZ) from the Coastal and Continental Shelf Zone (CCSZ; Jacobs 1986; 1991; Muench and Gordon 1995). The Antarctic CCSZ has been observed to host high rates of productivity in the summer (e.g., Smith and Nelson 1990; Arrigo et al. 2008) as melting sea-ice supplies dissolved iron and increases water column stratification, yielding ideal conditions for phytoplankton growth (Lannuzel et al. 2008). Inputs of dissolved iron from continental shelf sediments and coastal runoff further elevate the ambient iron concentrations, such that the CCSZ seldom experiences iron-depletion (Klunder et al. 2014). As a result, the large phytoplankton blooms of the CCSZ can at

79   times almost completely deplete surface nitrate concentrations (Jennings et al. 1984; Hoppema et al. 2000; Henley

80   et al. 2017), supporting high rates of carbon export (Arrigo et al. 2008). In contrast, the OOZ is far less productive

81   due to deeper mixed layer depths (MLD) that lead to light limitation of phytoplankton, along with persistent iron-

82   deplete conditions (Klunder et al. 2011; De Jong et al. 2012). Here, surface nutrients are never fully consumed

83   and carbon export rates are low (Boyd et al. 2008; Boyd and Ellwood 2010; Klunder et al. 2011; De Jong et al.

84   2012).

85

86   On an annual basis, phytoplankton growth in the euphotic zone that is fuelled by nitrate supplied from below (i.e.,

87   "new production") must be balanced by the export of sinking organic matter into the ocean interior (i.e., "export

88   production"), thus driving CO_2 removal (Dugdale and Goering 1967; Eppley and Peterson 1979). By contrast,

89   phytoplankton growth supported by nitrogen (N) sources that are recycled in the euphotic zone, such as

90   ammonium and urea (i.e., "regenerated production"), results in no net removal of CO_2 to the deep ocean. The

91   biologically-driven flux of carbon from surface waters, termed the "biological pump", transfers CO_2 to the isolated

92   waters of the deep ocean, maintaining the atmospheric concentration of this greenhouse gas (Volk and Hoffert

93   1985). The high nutrient-low chlorophyll state of much of the Southern Ocean represents a "leak" in the ocean's

94   biological pump since by consuming mixed-layer nutrients more completely, phytoplankton could theoretically

95   lower atmospheric CO_2 (Sarmiento and Toggweiler 1984). Indeed, a leading hypothesis for the 80-100 ppm

96   decrease in atmospheric CO_2 that characterized the ice ages is more complete consumption of surface nutrients

97   (i.e., a more efficient biological pump) in the open Southern Ocean (Sigman and Boyle 2000; Sigman et al. 2010;

98   Martínez-García et al. 2014).

99

100   Since phytoplankton in the CCSZ of the Weddell Sea consume much of the nitrate supplied to the surface

101   (Jennings et al. 1984; Hoppema et al. 2000), they should, by mass balance, drive the export of a significant amount

102   of atmospheric CO_2 to depth, most of which will be subducted in newly-formed bottom waters to be sequestered

103   for >1000 years (Ito et al. 2010). Understanding the controls on biological nutrient utilization in the Weddell Sea,

104   particularly the CCSZ, is thus central to our understanding of its contribution to the Southern Ocean's role in

105   setting atmospheric CO_2. In general, phytoplankton growth in the Weddell Sea is regulated by the seasonal cycle

106   of sea-ice, with the associated availability of light and iron imposing the main constraints (El-Sayed and Taguchi

107   1981). In winter, sea-ice formation and wind-driven mixing supply high concentrations of nutrients to ASW

108   (Hoppema et al. 2007; 2015) that remain largely unconsumed due to the deep mixed layers and short days (Cota

109   et al. 1992; Scharek et al. 1994; Spiridonov et al. 1996). Relief from light limitation in spring and early summer

110   driven by increased water-column stratification from sea-ice melt combined with enhanced solar radiation leads

111   to the development of phytoplankton blooms. The size and duration of these blooms is ultimately dependent on

112   both macro- (e.g., nitrate and silicate) and micronutrient (e.g., iron) availability (Martin et al. 1991; Boyd 2004;

113   Boyd and Ellwood 2010; Llort et al. 2015).

114

115   Observations suggest that Weddell Sea phytoplankton blooms are initially dominated by smaller phytoplankton

116   (e.g., *Phaeocystis antarctica*; 2-6 μm) that are well-adapted to the low light conditions associated with the fairly

117   deep springtime mixed layers (Schoemann et al. 2005). The ability of these smaller cells to rapidly grow and

118   consume the available nutrients results in bloom initiation. However, their small size also means that *P. antarctica*

119   experience high rates of predation by microzooplankton and sink fairly slowly, which enhances their contribution

120   to the microbial loop and decreases their carbon export potential (Hansen et al. 1994; 1997). As the season

121   progresses, rising air temperatures leads to increased sea-ice melt and warmer sea surface temperatures (SST),

122   resulting in an increasingly stratified upper water column that provides optimal conditions for the growth of larger

123   phytoplankton such as diatoms (Goffart et al. 2000; Nissen and Vogt 2020). Diatoms tend to rely heavily on nitrate

124   as their dominant N source (Malone 1980; Lomas and Glibert 1999; Fawcett and Ward 2011; Glibert et al. 2016)

125   and are a major vector for carbon export in the Southern Ocean due to their rapid sinking rates that are facilitated

126   by biogenic silica ballasting (Tréguer et al. 2017). The seasonal shift in the Weddell Sea community from small,

127   non-silicified phytoplankton to larger, more heavily-silicified species is thus associated with a significant increase

128   in carbon export (Treguer and Jacques 1992; De Baar et al. 2005; Boyd et al. 2007). Sea-ice melt also supplies

129   high concentrations of dissolved iron to surface waters (up to 7 nM in the western Weddell Sea; Lannuzel et al.

130   2008; Klunder et al. 2014), alleviating phytoplankton from iron limitation and supporting a high degree of surface

131   nitrate drawdown (Klunder et al. 2011, 2014). Eventually, as surface iron (and occasionally, nitrate; Hoppema, et

132   al., 2000) concentrations again become limiting, phytoplankton rely proportionally more on ammonium and other

133   regenerated N sources that have become increasingly available due to heterotrophic processing of the accumulated

134   (i.e., bloom) biomass (Goeyens et al. 1995; Semeneh et al. 1998). The phytoplankton community consequently

135   shifts once more towards smaller species that are better adapted to low iron conditions and specialize in the

136   consumption of regenerated N, ultimately leading to a decrease in carbon export (Goeyens et al. 1995).

137

138   The Weddell Sea is particularly understudied near LCIS where thick sea-ice conditions persist year-round. To our

139   knowledge, the only biogeochemical study conducted in the vicinity of LCIS was undertaken in the austral

140   summer of 1992/3. Using measurements of nutrient depletion, Hoppema et al. (2000) estimated primary

141   production in the vicinity of LCIS to be 47.5-95 mmol C m^{-2} d^{-1}, while in the central Weddell Sea it was

142   substantially lower at 8.3 mmol C m^{-2} d^{-1}. However, the study did not characterize the phytoplankton community,

143   so the extent to which phytoplankton diversity may have influenced primary production and nutrient drawdown

144   cannot be surmised. To evaluate the summertime fertility of the Weddell Sea and the potential importance of

145   different phytoplankton groups for carbon production and export, we directly measured the rates of total, new,

146   and regenerated production in the western Weddell Sea (predominantly at LCIS), as well as at Fimbul Ice Shelf

147   (FIS) in the south-eastern Weddell Sea. Rates of nitrification were also quantified to account for any nitrate

148   regenerated within the euphotic zone at the time of sampling as this N flux supports regenerated rather than new

149   production (e.g., Yool et al. 2007; Peng et al. 2018; Mdutyana et al. 2020). We interpret our rate data in the context

150   of concurrent measurements of regional hydrography, macronutrient concentrations and ratios, and phytoplankton

151   community composition.

152

153   **2. Methods**

154   **2.1. Field collections**

155   Sampling was conducted in the austral summer of 2018/2019 during the Weddell Sea Expedition onboard the R/V

156   *SA Agulhas II*. A total of 19 stations were sampled across the Weddell Sea and are categorised based on their

157   geographic position as Antarctic Peninsula (AP), Larsen C Ice Shelf (LCIS), Weddell Gyre (WG), or Fimbul Ice

158   Shelf (FIS) stations (Table 1; Figure 1). Hydrographic data were collected using a Seabird conductivity-

159   temperature-depth (CTD) profiler equipped with a photosynthetically active radiation (PAR) sensor. Density

160   (sigma-theta; σ_θ) was derived from CTD measurements of temperature, salinity and pressure, and was used to

161   identify the water masses present. At all stations, the mixed layer depth (MLD) was determined as the depth at

162   which the Brunt-Väisälä frequency squared (N^2; a function of σ_θ) reached a maximum (Schofield et al. 2015;

163   Carvalho et al. 2017).

164
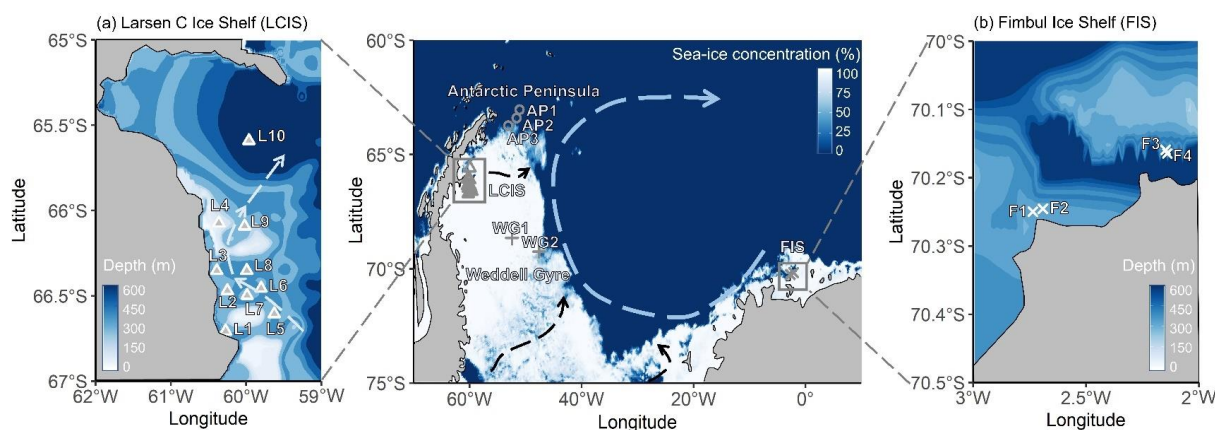
165   **Figure 1.** Maps of the Weddell Sea, Larsen C Ice Shelf (LCIS; insert a) and Fimbul Ice Shelf (FIS; insert b)
166   showing the position of the stations where rate experiments were conducted during the Weddell Sea Expedition
167   in January/February 2019. The symbols represent the different regions of the Weddell Sea sampled during the
168   expedition (circle – Antarctic Peninsula (AP); cross – FIS; triangle – LCIS; plus sign – Weddell Gyre (WG)). The
169   general cyclonic circulation of the Weddell Gyre (dashed blue arrow) is illustrated on the central map, and the
170   dashed black arrows indicate the input of modified water masses from Filchner-Ronne Ice shelf (FRIC) and LCIS
171   (Gordon et al. 1993; Schröder et al. 2002; Schodlok et al. 2002). The hypothesized circulation at LCIS (Nicholls
172   et al. 2004; Hutchinson et al. 2020) is shown by the dashed blue arrow in insert (a). The 3.125 km sea-ice
173   concentration data shown in the central panel were taken from ftp://ftp-projects.cen.uni-
174   hamburg.de/seaice/AMSR2/3.125km and the bathymetry data (inserts a and b) were taken from ETOPO1 (NOAA
175   National Geophysical Data Center 2009).

176

177   Seawater was collected from discrete depths using a rosette of twenty-four 12 L Niskin bottles. At each CTD

178   station, seawater samples for nutrient analysis were collected throughout the water column (typically at 15 discrete

179   depths), while samples for phytoplankton taxonomy and rate experiments were taken from 3-6 depths (see below)

180   that were selected based on profiles of temperature, fluorescence and PAR measured during the CTD down-casts.

181

182   Simulated *in situ* experiments were conducted to determine the rates of net primary production (NPP), N uptake

183   (as nitrate (NO_3^-), ammonium (NH_4^+), and urea-N), and nitrite (NO_2^-) oxidation (a measure of nitrification). For

184   NPP and N uptake, seawater was collected from three depths coinciding with the 55%, 10% and 1% PAR levels,

185   then pre-screened through a 200 µm mesh to remove large grazers and transferred to six 1 L and six 2 L

186   polycarbonate bottles per depth. ^{15}N-labeled NO_3^-, NH_4^+, or urea-N was added to four of the twelve bottles (i.e.,

187   two 1 L and two 2 L bottles per N species) and $NaH^{13}CO_3$ was added to the bottles amended with ^{15}N-NH_4^+. The

188   tracers were added at ~5-10% of the assumed ambient concentrations, yielding final concentrations in each bottle

189   of approximately 100 µM $NaH^{13}CO_3$, 1 µM ^{15}N-NO_3^-, 0.05 µM ^{15}N-NH_4^+, and 0.1 µM ^{15}N-urea-N. Bottles were

190   incubated on the deck for 4-6 hours in a custom-built incubator that was cooled with running surface (~7 m)

191   seawater and equipped with neutral density filters to simulate the relevant light levels. Experiments were

192   terminated via filtration onto 0.3 µm combusted (450°C for 8 hours) glass fibre filters (Sterlitech GF-75) that were

193   stored frozen in combusted (500°C for 5 hours) foil envelopes at -80˚C pending analysis.

194

195   Seawater samples for the NO_2^- oxidation experiments were collected from the 55%, 10% and 1% light levels, just

196   below the MLD, and at 200 m and 500 m. From each depth, seawater was transferred into duplicate 250 mL

197   opaque high-density polyethylene (HDPE) bottles to which ^{15}N-NO_2^- was added to achieve a final tracer

198   concentration of 0.1 µM. An initial 50 mL subsample ($T_{initial}$) was collected from each HDPE bottle immediately

199   following tracer addition and frozen at -20°C until analysis ashore. The 55%, 10%, 1% and MLD sample bottles

200   were incubated in the on-deck incubator for 20-30 hours while the 200 m and 500 m samples were incubated in a

201   ~2°C cold room. The experiments were terminated by collection and freezing of 50 mL T_{final} subsamples.

202

203   2.2. Nutrients

204   2.2.1. Nutrient concentration analysis

205   NO_3^-+NO_2^- and silicic acid (Si(OH)$_4$) concentrations were measured using a Lachat QuickChem flow injection

206   analysis platform following published auto-analysis protocols (Diamond 1994; Grasshoff 1976) in a configuration

207   with a detection limit of 0.5 µM. Duplicate samples were measured for NO_3^-+NO_2^- and Si(OH)$_4$ on different days,

208   and the standard deviation for duplicates was ≤0.5 µM, with a lower standard deviation for lower-concentration

209   samples. NO_3^- concentrations were determined by subtraction of NO_2^- from NO_3^-+NO_2^-. Concentrations of

210   phosphate (PO_4^{3-}) and NO_2^- were measured shipboard by standard benchtop colourimetric methods (Strickland

211   and Parsons 1968; Bendschneider et al. 2020; Parsons et al. 1984) using a Thermo Scientific Genesis 30 Visible

212   spectrophotometer. The detection limit was 0.05 µM and the standard deviation for duplicate samples was ≤0.05

213   µM. Aliquots of a certified reference material (JAMSTEC; Lot CG) were analysed during autoanalyser and

214   manual runs to ensure measurement accuracy.

215

216   NH_4^+ concentrations were measured shipboard following the fluorometric method of Holmes et al. (1999) using

217   a Turner Designs Trilogy fluorometer equipped with a UV module. The detection limit was <0.05 µM and the

218   standard deviation for duplicate samples was ≤0.05 µM. The matrix effect (ME) that results from the calibration

219   of seawater samples with Milli-Q water standards was calculated using the standard addition method (Saxberg

220   and Kowalski 1979). All samples were corrected for the ME (Taylor et al. 2007), which was always <10% and

221   typically ≤5%. Urea-N concentrations were measured following the colourimetric method of Revilla et al. (2005)

222   using a Thermo Scientific Genesis 30 Visible spectrophotometer equipped with either a 1 cm- or 5 cm-pathlength

223   cell. The detection limit was 0.05 µM and the standard deviation for duplicate samples was ≤0.05 µM. Hereafter,

224   we use "urea" when referring to urea-N.

225

226   2.2.2. Estimating nutrient depletion

227   The net decrease in euphotic zone nutrient concentrations following nutrient recharge in winter (i.e., the extent of

228   nutrient depletion due to consumption by phytoplankton), between the start of the growing season until the time

229   of our sampling, can be estimated for each station as:

230

231 $$X\ depletion = [X]_{measured} - [X]_{source} \qquad (1)$$

232

233 where $[X]_{source}$ is the average $[NO_3^-]$, $[Si(OH)_4]$ or $[PO_4^{3-}]$ in winter water (WW; a shallow temperature minimum

234 layer underlying ASW that is the remnant of the winter surface mixed layer and considered representative of the

235 pre-bloom surface conditions) and $[X]_{measured}$ is the measured nutrient concentration (Le Corre and Minas 1983;

236 Jennings et al. 1984; Goeyens et al. 1995; Rubin et al. 1998; Hoppema et al. 2007).

237

238 Seasonal melting of sea-ice in the Weddell Sea introduces low-salinity, low-nutrient waters to the mixed layer

239 (Eicken 1993), potentially leading to an overestimate of phytoplankton-driven nutrient depletion. We thus correct

240 X depletion for the effect of ice melt as:

241

242 $$X\ depletion_{(corrected)} = X\ depletion - X\ depletion_{(melt\ water)} \qquad (2a)$$

243

244 where $X\ depletion_{(melt\ water)}$ is the decrease in the surface $[NO_3^-]$, $[Si(OH)_4]$ or $[PO_4^{3-}]$ due to sea-ice melt (i.e., the

245 dilution effect), calculated as:

246

247 $$X\ depletion_{(melt\ water)} = [X]_{source} - [X]_{melt\ water} \qquad (2b)$$

248

249 where: $$[X]_{melt\ water} = [X]_{sea-ice}\,(f_{sea-ice}) + [X]_{source}(1-f_{sea-ice}) \qquad (2c)$$

250

251 Here, the nutrient concentrations in summertime sea-ice ($[X]_{sea-ice}$) are assumed to be: $[NO_3^-]_{sea-ice} = 1$ μM,

252 $[Si(OH)_4]_{sea-ice} = 5$ μM, and $[PO_4^{3-}]_{sea-ice} = 0.3$ μM (Fripiat et al. 2014), and:

253

254 $$f_{sea-ice} = \frac{salinity_{measured} - salinity_{source}}{salinity_{measured} - salinity_{sea-ice}} \qquad (2d)$$

255

256 with salinity$_{sea-ice}$ taken to be 5 based on measurements made during the cruise and salinity$_{source}$ set to 34.2 at FIS

257 and 34.4 at the other stations (the salinity of WW; Figure 2c insert). On average, correcting for sea-ice melt

258 changed the estimates of X depletion by $0.4 \pm 0.9\%$.

259

260 The approach outlined above for calculating $X\ depletion_{(corrected)}$ assumes, following correction for sea-ice melt,

261 that nutrient drawdown is due to phytoplankton assimilation only, a reasonable assumption in the Weddell Sea in

262 summer.

263

264 **2.3. Uptake rates**

265 Incubation filters were oven-dried for 24 hours at 40°C, then folded into tin cups. Samples were analysed using a

266 Flash Elemental Analyser 1112 Series coupled to a Delta V Plus isotope ratio mass spectrometer (IRMS) in a

267 configuration with a detection limit of 2 μg C and 1 μg N. Blanks (combusted unused filters + tin cups) and

268 laboratory running standards, calibrated to certified IAEA reference materials, were run after every five samples.

269

270   The specific rates of carbon fixation (V_C) and NO_3^-, NH_4^+ and urea uptake ($V_{NO_3^-}$, $V_{NH_4^+}$, V_{urea}; d^{-1}) were calculated

271   according to equation 2 in Dugdale and Wilkerson (1986). NPP and the absolute rates of NO_3^-, NH_4^+ and urea

272   uptake (ρNO_3^-, ρNH_4^+ and $\rho urea$; μM d^{-1}) were then determined by multiplying V_C by the concentration of

273   particulate organic carbon ([POC]) and $V_{NO_3^-}$, $V_{NH_4^+}$ and V_{urea} by the concentration of particulate organic nitrogen

274   ([PON]) (Dugdale and Wilkerson 1986; equation 3).

275

276   **2.4. NO_2^- oxidation rates**

277   The $T_{initial}$ and T_{final} samples collected from the NO_2^- oxidation incubations were measured for the $\delta^{15}N$ of NO_3^-

278   ($\delta^{15}N_{NO3}$; where $\delta^{15}N = ((^{15}N_{sample}/^{14}N_{sample})/(^{15}N_{standard}/^{14}N_{standard}) - 1) \times 1000$) using the denitrifier method (Sigman

279   et al. 2001; McIlvin and Casciotti 2011). Prior to isotopic analysis, all samples were treated with sulfamic acid to

280   remove NO_2^- as the denitrifier method converts both NO_2^- and NO_3^- to N_2O gas (Granger and Sigman 2009); the

281   difference in $\delta^{15}N_{NO3}$ between the T_{final} and $T_{initial}$ samples was then taken as the $^{15}NO_3^-$ enrichment due to $^{15}NO_2^-$

282   oxidation (Peng et al. 2015). Results were referenced to atmospheric N_2 using certified reference materials (IAEA-

283   NO-3, USGS-34, and USGS-32; Gonfiantini 1984; Böhlke and Coplen 1995; Böhlke et al. 2003). The rate of

284   NO_2^- oxidation ($V_{NO_2^-}$; nM d^{-1}) was calculated following Peng et al. (2015) as:

285

286    $$V_{NO_2^-} = \frac{\Delta[^{15}NO_3^-]}{f_{NO_2^-}^{15} \times t} \tag{3}$$

287

288   where $\Delta[^{15}NO_3^-]$ is the difference in the concentration of $^{15}NO_3^-$ between the end and the start of the experiment

289   (i.e., $T_{final} - T_{initial}$) due to NO_2^- oxidation, $f_{NO_2^-}^{15}$ is the fraction of $^{15}NO_2^-$ at the start of the incubation, and t is the

290   length of the incubation (days). The detection limit for $V_{NO_2^-}$ ranged from 0.06-0.46 nM d^{-1} (calculated following

291   Santoro et al. 2013). We take $V_{NO_2^-}$ as an appropriate measure of the nitrification rate given that NO_2^- oxidation is

292   the step in the nitrification pathway that produces NO_3^-.

293

294   To determine relative carbon export potential at each station, we calculated the f-ratio (a measure of new

295   production relative to total (i.e., new+regenerated) production) using the absolute N uptake and NO_2^- oxidation

296   rates and a modified version of the Eppley and Peterson (1979) equation:

297

298    $$\text{f-ratio}_{(excluding\ urea)} = \frac{\rho NO_3^- - V_{NO_2^-}}{\rho NO_3^- + \rho NH_4^+} \tag{4a}$$

299

300    $$\text{f-ratio}_{(including\ urea)} = \frac{\rho NO_3^- - V_{NO_2^-}}{\rho NO_3^- + \rho NH_4^+ + \rho urea} \tag{4b}$$

301

302   Equation 4 accounts for euphotic zone nitrification ($V_{NO_2^-}$), which yields regenerated rather than new NO_3^- that is

303   then available for phytoplankton to consume. Not accounting for $V_{NO_2^-}$ could result in the f-ratio being

304   overestimated. Equation 4b accounts for urea uptake, that was either measured (at the LCIS stations and WG1) or

305   calculated (at the AP, FIS and WG2) using equation 7 (see section 3.3.4 below).

306

2.5. Phytoplankton taxonomy and carbon biomass

At all stations, microphytoplankton samples were collected between the surface and 30 m using a HYDROBIOS conical plankton net (r = 12.5 cm; h = 50 cm) with a mesh size of 55 μm. Samples were transferred to 50 mL centrifuge tubes, fixed with 10 μL of 25% glutaraldehyde and stored at room temperature in the dark until later analysis via light and scanning electron microscopy. Additionally, samples for flow cytometry were collected in 50 mL centrifuge tubes from Niskin bottles fired at the 55%, 10% and 1% light depths. These samples were fixed with 10 μL of 25% glutaraldehyde and stored at 4°C until analysis.

In the onshore laboratory, each preserved net-sample was homogenized, and one drop (40 μL) was wet mounted on a slide. All the cells on the slide with intact chloroplasts (i.e., alive at the time of sampling) were counted at 400x or 630x magnification using a Zeiss AxioScope A1 light microscope (LM). The number of cells/L was calculated as:

$$\text{cells per litre} = A \left(\frac{1}{L}\right)\left(\frac{n}{V}\right) \tag{5}$$

where A = number of cells per drop; L = volume of water sampled (1470 L; computed using the volume of a cylinder, $\pi\, r^2 h$, where r = 0.125 m and h = 30 m depth); n = volume of the concentrated sample; and V = volume of 1 drop.

An aliquot of 5 mL from each preserved sample was cleaned by removing carbonate particles and organic matter using 10% hydrochloric acid and 37% hydrogen peroxide, respectively. After thorough rinsing with distilled water, permanent slides were prepared by pipetting the cleaned material onto acid-washed coverslips, air drying overnight and mounting the cover slips onto glass slides using Naphrax® mountant (refractive index = 1.7). The permanent slides were examined using a Zeiss AxioScope A1 LM equipped with differential interference contrast (DIC) at 1000x magnification (under oil immersion) for identification of the diatom cells to the lowest taxonomic classification possible. Stubs were also prepared from the cleaned material for Scanning Electron Microscopy (SEM), with a JEOL JSM 7001F field emission SEM used to visualize the morphological features not evident under LM.

The average size (μm) and carbon content (pg C cell^{-1}) of each identified diatom species was taken from Leblanc et al. (2012) for high latitude locations (50 – 70°S) (Table S1), and the carbon content of colonial *P. antarctica* was estimated as 13.6 pg C cell^{-1} (Mathot et al. 2000) for single cells within a colony. Since the majority of *P. antarctica* were in spherical colony form, the total colony carbon biomass (C$_{COL}$) was calculated as:

$$C_{COL} = [13.60 \text{ x } N_C] + C_M \tag{6}$$

where N_C is the number of cells counted per litre; C_M is the mucus-related carbon calculated as $C_M = 0.213$ x $V_{COL} + 4.58$; and V_{COL} is the volume of the spherical colony, calculated as $V_{COL} = 417$ x $N_C^{1.67}$ (Mathot et al. 2000).

347 All flow cytometry samples were analyzed using a BD LSR II SORP flow cytometer with blue/red/green laser
348 configuration. Prior to analysis, sample tubes were gently agitated to homogenize the contents, then 1 mL of
349 sample was transferred to a 5 mL polycarbonate test tube. The size-class to which each cell belonged was defined
350 based on its forward scatter area (FSC-A) relative to the FSC-A of 2.8 μm and 20 μm beads (Figure S1a). Once
351 categorized as either picoplankton (<2.8 μm), nanoplankton (2.8-20 μm) or microplankton (>20 μm), the cells
352 were grouped into six populations based on their orange fluorescence (indicative of phycoerythrin; PE) relative
353 to their red fluorescence (indicative of chlorophyll-a; chl-a): two *Synechococcus* populations (Syn 1 and Syn 2),
354 one picoeukaryote population (PicoEuk), two nanoeukaryote populations (NanoEuk 1 and NanoEuk 2), and one
355 microeukaryote population (MicroEuk; see section S2 in the Supplemental Information for details of population
356 identification). The biovolumes of the eukaryotic populations were estimated based on their FSC-A relative to
357 that of six beads of known size and volume (Figure S1c; Table S2). *Synechococcus* had an unrealistically high
358 FSC-A, which is an artefact of this group having a high ratio of photosystem I to photosystem II compared to the
359 other phytoplankton populations. This increases electron chain activity, leading to an increase in the emission
360 spectrum and low excitation of the *Synechococcus* populations (Kaprelyants and Kell 1993; Sunda and Huntsman
361 2015). The biovolume of *Synechococcus* was thus assumed to be 1 μm^3 (Kana and Glibert 1987; Paulsen et al.
362 2015). Biovolume is taken here as a proxy for biomass.
363
364 **3. Results**
365 **3.1. Water column hydrography**
366 Throughout the study region, relatively cool and fresh (-2 to 0°C and 33.0 to 34.5) ASW occurred between the
367 surface and 135 m (Figure 2). Through this layer and down to 200 m, salinity increased with depth while
368 temperature decreased, reaching a local minimum (-1.6°C) at ~100 m. These hydrographic changes are
369 characteristic of WW, which is considered a summertime record of winter conditions and a reflection of the initial
370 state from which the mixed layer evolves over the spring/summer growing season (Altabet and Francois 2001).
371 Below WW at the AP and WG stations, salinity remained constant while temperature increased with depth,
372 reaching a local maximum (0.5°C) at 500 m and 300 m for the AP and WG, respectively. This feature is
373 characteristic of Warm Deep Water (WDW), a temperature maximum layer that is a modified form of Circumpolar
374 Deep Water (CDW) (Muench and Gordon 1995; Fahrbach et al. 1995). Below WW at the LCIS and FIS stations,
375 salinity increased and temperature decreased with depth, reaching a local salinity maximum (34.6 at LCIS and
376 34.3 at FIS) and temperature minimum (≤ -1.8°C). The increase in salinity is characteristic of High Salinity Shelf
377 Water (HSSW) produced by brine rejection during sea-ice formation, while the decrease in temperature is
378 characteristic of Ice Shelf Water (ISW) produced by the supercooling of ASW under the ice shelves (Fahrbach et
379 al. 1995; Nicholls et al. 2009; Hutchinson et al. 2020). The densities of WW, WDW, HSSW and ISW are
380 contiguous, with the mixed product of these waters termed Modified Warm Deep Water (MWDW) (Fahrbach et
381 al. 1995). Below WDW at the AP and WG stations, temperature decreased due to the presence of Weddell Sea
382 Deep Water (WSDW; temperature range of -0.7 to 0°C) and Weddell Sea Bottom Water (WSBW; temperature ≤
383 -0.7°C) (Fahrbach et al. 1995; Muench and Gordon 1995).
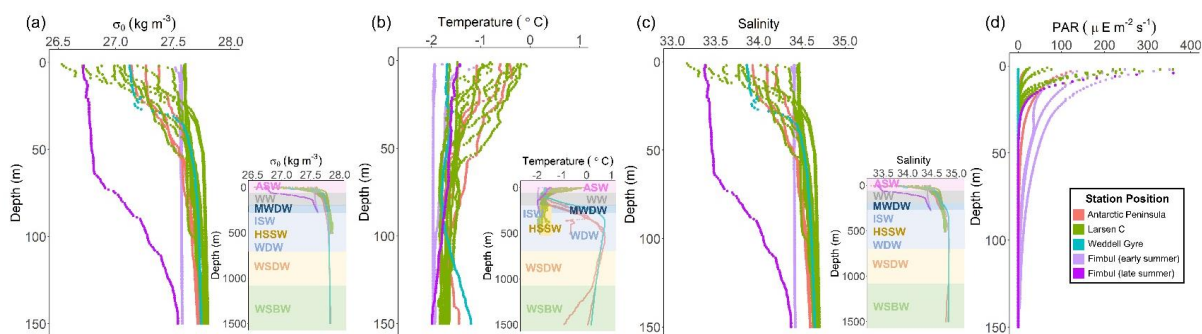384
385 Variability in the density of ASW was observed among the stations (Figure 2a). The surface density profiles at
386 the AP, WG and early-summer FIS stations were very similar, while the late-summer density profile at FIS

387 revealed lower-density waters over the upper 100 m. At LCIS, the surface density profiles were highly variable,

388 and no consistent pattern was observed, although the most northern stations (L9 and L10; Figure 1) were

389 characterised by the lowest densities. Stations L1 and L3, situated closest to the ice shelf, were characterised by

390 the highest densities, contiguous with the underlying WW layer.

391

392 The MLD appeared most strongly controlled by salinity at all stations and was always shallower than the depth

393 of the euphotic zone (Z_{eu}; Table 1), the latter defined as the depth to which 1% of surface PAR penetrated (Kirk

394 1994). The deepest MLD and Z_{eu} were observed at FIS in early summer (average MLD of 103 ± 36.6 m and Z_{eu}

395 of 91.7 ± 14.4 m; n = 3), while the shallowest MLD and Z_{eu} were observed at LCIS (average MLD of 13.9 ± 5.9

396 m and Z_{eu} of 28.5 ± 9.1 m; n = 10) (Figure 2d; Table 1). The rates of NPP, N uptake and nitrification were therefore

397 trapezoidally-integrated to Z_{eu} rather than to the MLD since we assume that phytoplankton were active at least to

398 the depth of 1% PAR.

Figure 2. Depth profiles (0-100 m) of (a) potential density (σ_0), (b) potential temperature, (c) absolute salinity, and (d) photosynthetically active radiation (PAR) at all stations. The inserts in panels (a), (b) and (c) show the profiles down to 1500 m, with the various water masses present at each station identified from their temperature and salinity ranges (WSBW – Weddell Sea Bottom Water, WSDW – Weddell Sea Deep Water, WDW – Warm Deep Water, MWDW – Modified Warm Deep Water, ISW – Ice Shelf Water, HSSW – High Salinity Shelf Water, WW – Winter Water, ASW – Antarctic Surface Water). The station positions are indicated by the different colours: red – Antarctic Peninsula, green – Larsen C Ice Shelf, blue –Weddell Gyre, light purple – early summer Fimbul Ice Shelf, and dark purple – late summer Fimbul Ice Shelf.

3.2. Nutrient concentrations

409 The concentrations of the regenerated N forms (i.e., NH_4^+ and urea) were generally low in the surface and

410 increased with depth to reach a maximum below Z_{eu}, before decreasing again to below detection by 200-300 m

411 (Figure 3a and b; Table 1). A sharp maximum in the NH_4^+ concentration was observed at Z_{eu} at all stations,

412 indicative of the depth of maximum net remineralisation. Urea was more variable, likely due to variability in the

413 processes that produce this N form (e.g., bacterial excretion; Berges and Mulholland 2008). The highest average

414 concentrations of regenerated N in the euphotic zone were observed at LCIS and FIS in late summer (0.62 ± 0.30

415 μM for NH_4^+ and 0.21 ± 0.07 μM for urea), while the lowest concentrations were observed at FIS in early summer

416 (below detection for both NH_4^+ and urea). Elevated regenerated N concentrations were also observed at the AP

417 stations (euphotic zone average of 0.8 ± 0.3 μM for NH_4^+ and 0.2 ± 0.06 μM for urea), while low concentrations

418 were observed at the WG stations (euphotic zone average of 0.3 ± 0.1 μM for NH_4^+ and 0.1 ± 0.0 μM for urea).

419

420   The concentrations of NO_2^- were generally low throughout the euphotic zone, and decreased to below detection

421   by 120 m at the FIS, AP, and WG stations (with the exception of a single sample from the early-summer FIS),

422   and by 500 m at LCIS (Figure 3c). A high degree of variability was observed, with the highest surface-layer NO_2^-

423   concentrations occurring in the WG and at FIS in late summer (average euphotic zone NO_2^- concentrations of 0.08

424 $\pm$ 0.06 µM and 0.12 $\pm$ 0.03 µM, respectively).

425
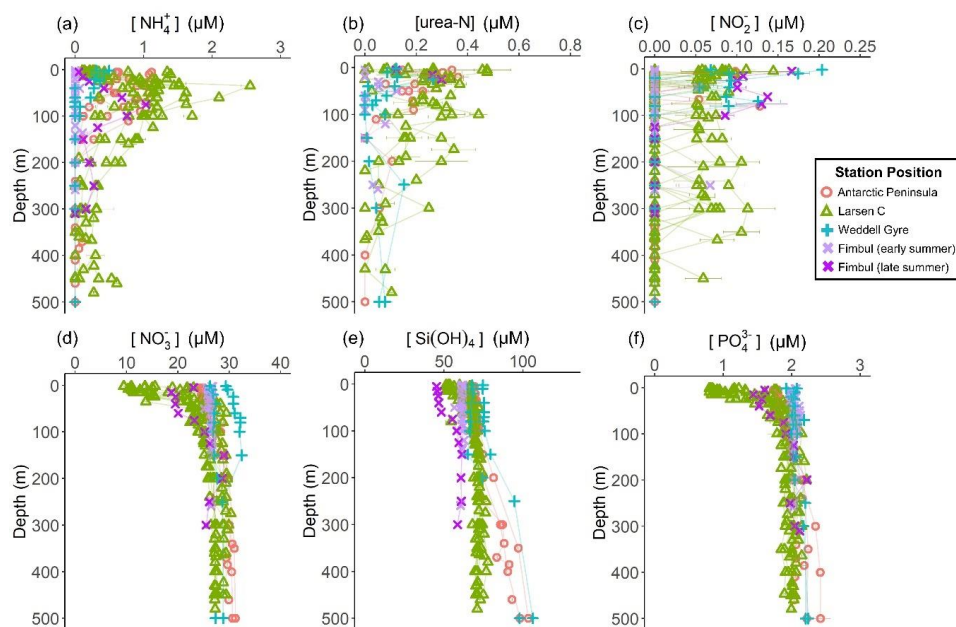
426

427

Figure 3. Depth profiles (0-500 m) of the concentrations of (a) NH_4^+, (b) urea-N, (c) NO_2^-, (d) NO_3^-, (e) $Si(OH)_4$
and (f) PO_4^{3-}. For all panels, the error bars represent $\pm$ 1 SD replicate samples (n = 2-3). Where applicable, the
error has been propagated according to standard statistical practices.

432   The euphotic zone concentrations of NO_3^-, $Si(OH)_4$ and PO_4^{3-} decreased towards the surface due to assimilation

433   by phytoplankton (Figure 3d-f). The lowest surface concentrations of NO_3^- and PO_4^{3-} were observed at LCIS (16.6

434   $\pm$ 3.8 µM and 1.3 $\pm$ 0.4 µM, respectively) and of $Si(OH)_4$ was observed at FIS in late summer (46.1 $\pm$ 0.8 µM).

435   The highest surface concentrations of NO_3^-, PO_4^{3-} and $Si(OH)_4$ occurred in early summer at FIS (26.5 $\pm$ 0.32 µM,

436   2.0 $\pm$ 0.04 µM and 61.6 $\pm$ 0.5 µM, respectively). Elevated $Si(OH)_4$ and PO_4^{3-} concentrations were observed

437   between 200 and 500 m at the AP and WG stations due to the presence of WDW at these stations versus shelf

438   waters (i.e., ISW and HSSW) at LCIS and FIS. WDW has the longest residence time of all water masses in the

439   Weddell Sea, and has therefore undergone the greatest modification by physical and biogeochemical processes

440   (Whitworth and Nowlin 1987; Hoppema et al. 2015). The depth of maximum remineralisation in the open Weddell

441   Sea is 300-500 m, the depth range occupied by WDW (Vernet et al. 2019, and references therein). The high rates

442   of remineralisation, and therefore nutrient accumulation, in WDW account for the elevated nutrient concentrations

443   observed in WDW relative to the shelf water masses (Whitworth and Nowlin 1987). Estimates of NO_3^-, $Si(OH)_4$

444   and PO_4^{3-} depletion (i.e., X depletion$_{(corrected)}$; equation 2) were highest at LCIS (average NO_3^- depletion of 8.3 $\pm$

445 3.9 µM, $Si(OH)_4$ depletion of 8.3 ± 4.0 µM and PO_4^{3-} depletion of 0.6 ± 0.3 µM), while the lowest nutrient

446 depletions occurred in early summer at FIS (average NO_3^- depletion of 0.3 ± 0.3 µM, $Si(OH)_4$ depletion of 0.6 ±

447 0.6 µM and PO_4^{3-} depletion of 0.00 ± 0.02 µM) (Figure 4a-c; Table 1).

448
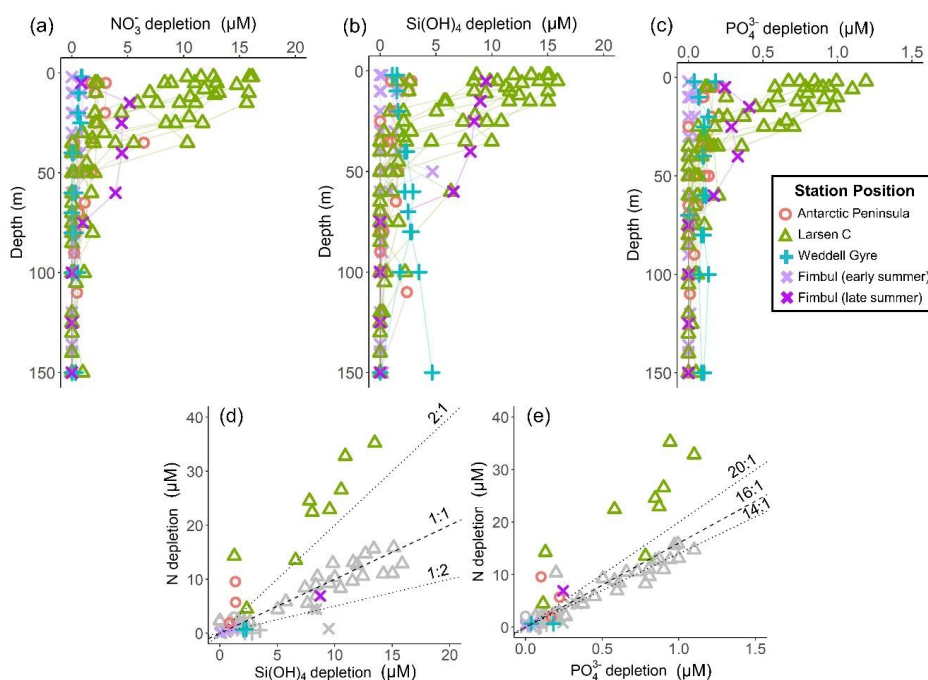
449

450 **Figure 4.** Depth profiles (0-150 m) of (a) NO_3^- depletion, (b) $Si(OH)_4$ depletion and (c) PO_4^{3-} depletion at each
451 station. Also shown are scatterplots of (d) $Si(OH)_4$ depletion versus NO_3^- depletion at each depth over the euphotic
452 zone at all stations (grey symbols) and the theoretical euphotic zone-averaged $Si(OH)_4$ versus total N depletion
453 (coloured symbols; see text for details) and (e) PO_4^{3-} depletion versus NO_3^- depletion at each depth over the
454 euphotic zone at all stations (grey symbols) and the theoretical euphotic zone-averaged PO_4^{3-} versus total N
455 depletion (coloured symbols). The dashed line in panel (d) represents the 1:1 Si:N depletion ratio, expected for
456 iron-replete diatoms (Ragueneau et al. 2000; Hutchins and Bruland 1998; Takeda 1998; Mosseri et al. 2008),
457 while the dotted lines represent the 1:2 Si:N ratio, indicative of enhanced activity of non-siliceous phytoplankton,
458 and the 2:1 Si:N ratio, expected for iron-limited diatoms (Arrigo et al. 1999; Franck et al. 2000; Brzezinski et al.
459 2003; Green and Sambrotto 2006; Mosseri et al. 2008; Weber and Deutsch 2010; Martiny et al. 2013). The dashed
460 line in panel (e) represents the 16:1 N:P depletion ratio (the Redfield ratio), while the dotted lines represent the
461 20:1 N:P ratio, expected for *P. antarctica*, and 14:1 N:P ratio, expected for iron-replete diatoms (Hutchins and
462 Bruland 1998; Takeda 1998; Arrigo et al. 1999; Ragueneau et al. 2000; Mosseri et al. 2008).

463

464 Variations in the depletion ratios of $Si(OH)_4$:NO_3^- and NO_3^-:PO_4^{3-} can be used as indicators of the nutrient status

465 of the phytoplankton community, particularly diatoms. Under iron-replete conditions, diatoms have been observed

466 to consume $Si(OH)_4$ and NO_3^- in a ratio of ~1:1, and NO_3^- and PO_4^{3-} in a ratio of ~14:1 (Hutchins and Bruland

467 1998; Takeda 1998; Ragueneau et al. 2000; Mosseri et al. 2008), while under conditions of limitation, the ratio of

468 $Si(OH)_4$:NO_3^- uptake rises (to >>2:1) and NO_3^-:PO_4^{3-} uptake decreases (to as low as 10:1) (Arrigo et al. 1999;

469 Franck et al. 2000; Brzezinski et al. 2003; Green and Sambrotto 2006; Mosseri et al. 2008; Weber and Deutsch

470 2010; Martiny et al. 2013). Additionally, the dominance of one phytoplankton species over another may cause

471 deviations in the NO_3^-:PO_4^{3-} depletion ratio. For example, in regions dominated by *P. antarctica*, Arrigo et al.

472 (1999) observed a NO_3^-:PO_4^{3-} depletion ratio of ~20:1, while in those dominated by iron-deplete diatoms, it was

473 ~10:1. The NO_3^-:PO_4^{3-} depletion ratios can thus also yield insights into the dominant phytoplankton species active

474 in the upper water column. In our study, the average euphotic zone $Si(OH)_4$:NO_3^- depletion ratios ranged from 0.5

475 to 6.1 (Table 1), with the highest ratios estimated for the WG stations (average of 5.4 ± 5.5) and FIS stations F3

476 and F4 (average of 2.7 ± 2.8; the same station occupied in early- (F3) and late summer (F4)). The euphotic zone

477 average NO_3^-:PO_4^{3-} depletion ratios were more variable, ranging from 3.7 ± 1.5 to 48.6 ± 11.5, with the lowest

478 ratios computed for the WG stations (average of 4.1 ± 1.5) and the highest for FIS in early summer (average of

479 33.7 ± 3.6).

480

481 **3.3. Upper ocean biomass, NPP and N uptake rates**

482 **3.3.1. Particulate organic carbon and nitrogen**

483 The highest concentrations of POC and PON were observed in the surface at all stations (Figure 5a), decreasing

484 towards Z_{eu} (Figure 5e). Averaged over the euphotic zone, the lowest POC and PON concentrations occurred in

485 early summer at FIS (4.6 ± 1.5 µM and 0.3 ± 0.1 µM, respectively) and the highest at LCIS (17.9 ± 7.3 µM and

486 2.5 ± 0.8 µM, respectively; Table 2). Across the region, the biomass C:N ratio was fairly uniform throughout the

487 euphotic zone, except at stations F1, F2 and the WG stations (Figure 5b, d and f). In general, the FIS and WG

488 stations were characterized by significantly higher C:N ratios than those expected from Redfield stoichiometry

489 (C:N = 6.63:1), averaging 16.5 ± 8.8 and 12.3 ± 1.8, respectively. At the LCIS stations, the biomass C:N ratios

490 were close to the Redfield ratio (7.4 ± 1.9), while the AP stations were characterized by slightly higher C:N ratios

491 (8.3 ± 2.5).
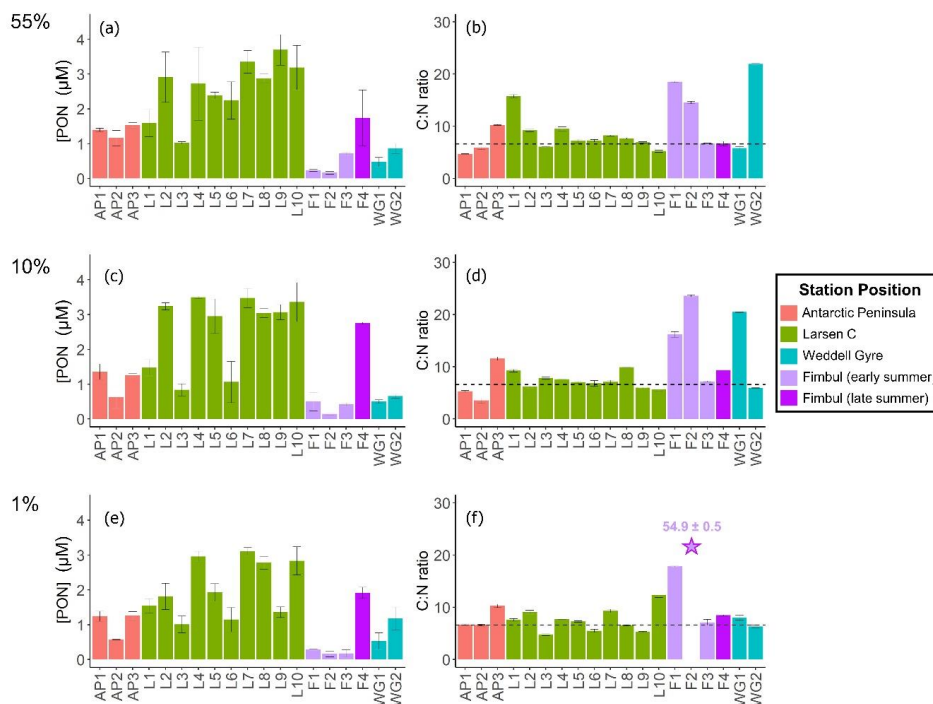
Figure 5. Bar plots of (a, c, e) PON concentrations and (b, d,f) biomass C:N ratios measured at the 55% (a-b), 10% (c-d) and 1% light levels (e-f). The dotted black line in panels (b), (d), and (f) indicates the Redfield C:N ratio of 6.63. The error bars represent ± 1 SD of replicate samples (n = 2-6). Where applicable, the error has been propagated according to standard statistical practices.

3.3.2. Rates of NPP and N uptake

At all stations, NPP was highest at the surface (Figure 6a) and decreased towards Z_{eu} (Figure 6i). The highest depth-specific rates were observed at LCIS (except at station L10 where the rates were very low), while the lowest rates occurred in early summer at FIS (with particularly low rates at station F1; Figure 6a, e and i). At the WG stations and at FIS in late summer, rates of NPP were comparable to the lower end of the rates observed at LCIS, while NPP along the AP increased shoreward to values similar to those at LCIS (i.e., the lowest rates were observed at AP1 and the highest at AP3). The highest euphotic zone-integrated rates of NPP were observed at AP3 (65.0 ± 0.1 mmol m^{-2} d^{-1}) and L5 (61.0 ± 0.7 mmol m^{-2} d^{-1}), while the lowest occurred at L10 (1.8 ± 0.04 mmol m^{-2} d^{-1}) (Table 2).

As per NPP, the rates of ρNO_3^- decreased towards Z_{eu} at all stations (Figure 6b, f and j), as did the extent of NO_3^- depletion (Figure 4a). The depth-specific rates of ρNO_3^- were highest at LCIS and lowest in early summer at FIS. However, because the euphotic zone was generally shallower at LCIS than at the other stations, the euphotic zone-integrated rates of ρNO_3^- were fairly similar across the study region, with the largest variability observed at LCIS (Table 2). In late summer at FIS, the rates of ρNO_3^- were on average higher than at LCIS (3.9 ± 0.03 mmol m^{-2} d^{-1} at F4 versus an average of 2.2 ± 1.1 mmol m^{-2} d^{-1} at LCIS), with depth-specific rates that were double those

Biogeosciences
Discussions

513   measured at FIS in early summer. The sea-ice at FIS had completely melted by late summer, which likely

514   contributed to the increase in ρNO_3^- later in the season. The highest euphotic zone-integrated rates of ρNO_3^- were

515   observed at stations F3 and L5 (4.8 ± 0.07 mmol m^{-2} d^{-1} and 4.7 ± 0.04 mmol m^{-2} d^{-1}, respectively). At L5, this

516   elevated rate coincided with low euphotic zone NO_3^- concentrations (12.0 ± 1.9 µM; Figure 3d) and a high degree

517   of NO_3^- depletion (10.9 ± 2.3 µM; Figure 4a). The lowest euphotic zone-integrated rates of ρNO_3^- occurred at

518   station L10 (0.5 ± 0.0 mmol m^{-2} d^{-1}).

519

520   Across all stations, rates of ρNH_4^+ increased with depth, reaching a maximum at Z_{eu} (Figure 6c, g and k). The

521   highest depth-specific rates of ρNH_4^+ were observed at LCIS and the lowest at FIS in early summer. Euphotic

522   zone-integrated rates of ρNH_4^+ at the AP stations were comparable to those observed at LCIS (regional average

523   of 3.3 ± 2.2 mmol m^{-2} d^{-1} and 2.5 ± 1.3 mmol m^{-2} d^{-1}, respectively), while the rates at the WG stations and at FIS

524   in late summer were comparable to the lower end of the LCIS rates (regional averages of 2.0 ± 0.2 mmol m^{-2} d^{-1}

525   at WG and 1.9 ± 0.0 mmol m^{-2} d^{-1} at FIS). The early- to late-summer rise in the euphotic zone-integrated rates of

526   ρNH_4^+ at FIS coincided with an increase in the average euphotic zone NH_4^+ concentration from below detection

527   to 0.2 ± 0.1 µM (Figure 3a). At the AP, LCIS and WG stations, the rates of ρNH_4^+ were similar to the coincident

528   rates of ρNO_3^-, while at FIS, ρNH_4^+ was less than half of ρNO_3^- (Table 2). The highest euphotic zone-integrated

529   rates of ρNH_4^+ were observed at station AP3 (5.8 ± 0.0 mmol m^{-2} d^{-1}), coincident with high average euphotic zone

530   NH_4^+ (1.1 ± 0 µM). The lowest euphotic zone-integrated rates occurred at station F1 (0.4 ± 0.0 mmol m^{-2} d^{-1})

531   where the concentration of NH_4^+ in the euphotic zone was below detection.

532

533   Rates of ρurea were only measured at the LCIS stations and WG1 (Figure 6d, h and l; Table 2). A high degree of

534   variability in the rates of ρurea was observed at LCIS, with euphotic zone-integrated rates ranging from 0.2 to 1.1

535   mmol m^{-2} d^{-1} (regional average of 0.6 ± 0.3 mmol m^{-2} d^{-1}). This variability appears to be related to the urea

536   concentrations, with the highest rates of ρurea occurring where the ambient urea concentrations were highest (e.g.,

537   station L5), and vice versa (e.g., station L4) (Figure 3b). On average, the rates of ρurea in the WG were half the

538   coincident rates of ρNH_4^+, and urea concentrations were low (Figure 3b; Table 2).
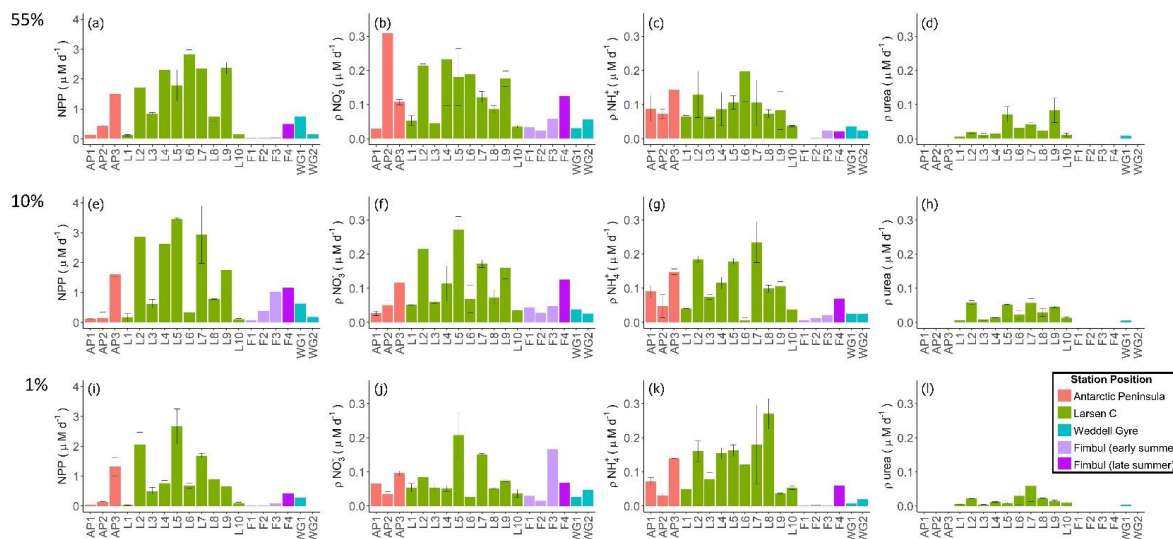
Figure 6. Daily rates of (a, e, i) NPP, (b, f, j) ρNO₃⁻, (c, g, k) ρNH₄⁺ and (d, h, l) ρurea for the 55% (a-d), 10% (e-h) and 1% light level (i-l). Where there are no bars in panels (d), (h) and (l), no data are available. The error bars represent ± 1 SD of replicate samples (n = 2).

3.3.3. Rates of nitrite oxidation

Rates of $V_{NO_2^-}$ were low throughout the euphotic zone across the study region (average of 20.8 ± 31.3 μmol m⁻² d⁻¹), equivalent to 0 to 3.6% (average of 0.7 ± 1.1%) of ρNO₃⁻, and rapidly increased below Z_{eu} (Figure 7). The highest euphotic zone rates were observed at WG1 (average of 6.3 ± 5.0 nM d⁻¹), while the lowest rates occurred at the AP (regional average of 0.0 ± 0.04 nM d⁻¹; Figure 7).
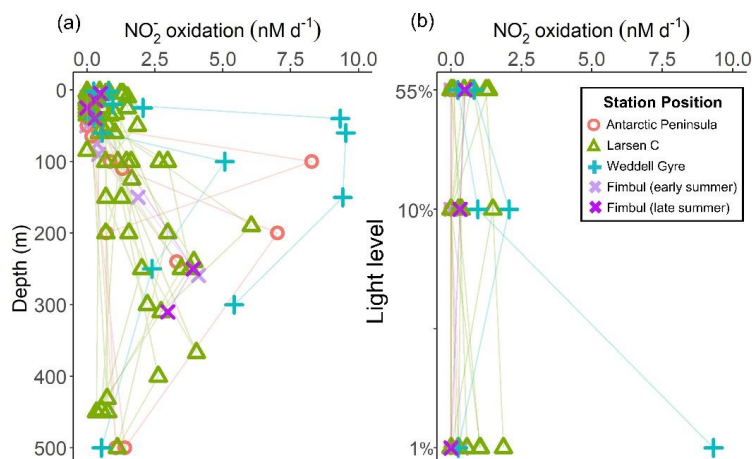
Figure 7. Depth profiles of the NO₂⁻ oxidation rates measured at each station (a) between the surface and 500 m, and (b) within the euphotic zone only.

552 **3.3.4. f-ratio estimates**

553 Urea uptake was measured at the LCIS stations and WG1 (at 11 out of 19 stations; Figure 6; Table 2) where it

554 accounted for 8 ± 6% of total N uptake (i.e., $\rho NO_3^- + \rho NH_4^+ + \rho urea$). Excluding urea uptake when calculating

555 the f-ratio would therefore overestimate the fraction of potentially exportable carbon by ~8%. We estimated urea

556 uptake at the stations where it was not measured as:

557

558 $$\rho urea = (\rho NO_3^- + \rho NH_4^+) \times 0.08 \tag{7}$$

559

560 Equation 7 may overestimate urea uptake at some of the stations, particularly where low urea concentrations were

561 measured. Theoretically, $\rho urea$ can also be estimated by assuming that total N uptake should equal NPP/6.63 (i.e.,

562 assuming balanced phytoplankton growth), such that any difference between $\rho NO_3^- + \rho NH_4^+$ and NPP/6.63 is due

563 to urea uptake. However, this approach underestimated urea uptake at all the stations where it was directly

564 measured. We therefore chose to use equation 7 to estimate urea uptake for the stations lacking $\rho urea$

565 measurements as this approach will yield a more conservative (i.e., lower) estimate of the fraction of potentially

566 exportable carbon. Figure 8 shows how including urea uptake affected the f-ratio throughout the sample region,

567 with the white (no urea uptake measured) and hashed bars (urea uptake measured) indicating the amount by which

568 the f-ratio decreased when urea uptake was included (i.e., equation 4b versus equation 4a).

569

570 The euphotic zone-integrated f-ratios were highest at FIS in early summer (average f-ratio$_{(excluding urea)}$ of 0.79 ±

571 0.1 and f-ratio$_{(including urea)}$ of 0.73 ± 0.09) and lowest at LCIS (average f-ratio$_{(excluding urea)}$ of 0.50 ± 0.09 and f-

572 ratio$_{(including urea)}$ of 0.47 ± 0.08) (Figure 8; Table 2). The variability in the f-ratios among stations appears to be

573 related to the availability of NH_4^+. For example, at FIS in early summer there was no NH_4^+ available to the

574 phytoplankton and the highest f-ratios were observed (average f-ratio$_{(excluding urea)}$ of 0.82 ± 0.08 and f-ratio$_{(including}$

575 $_{urea)}$ of 0.76 ± 0.07), while in late summer, NH_4^+ concentrations were elevated (0.2 ± 0.1 μM) and the f-ratio

576 declined (f-ratio$_{(excluding urea)}$ of 0.68 ± 0.16 and f-ratio$_{(including urea)}$ of 0.63 ± 0.15).
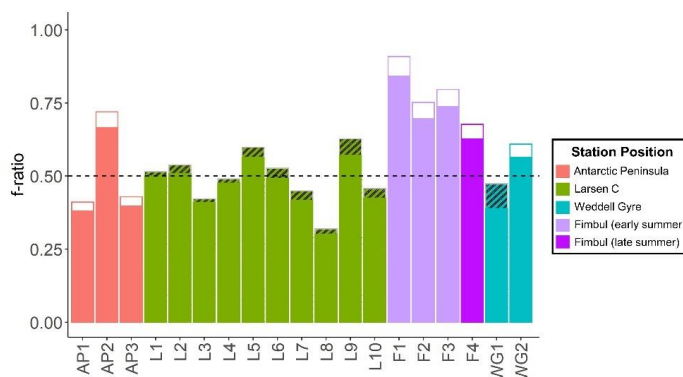
577

578 **Figure 8.** Euphotic zone-integrated f-ratios at each station. The hashed and white bars show the difference
579 between the f-ratio$_{(excluding urea)}$ (higher value) and the f-ratio$_{(including urea)}$ (lower value), with the hashed bars
580 representing the stations where urea uptake was measured and the white bars where it was estimated (see text for
581 details).

582

### 3.3.5. Phytoplankton community composition

584 The flow cytometry data suggest that the phytoplankton community was numerically dominated by picoplankton

585 at all stations, with *Synechococcus* emerging as the most abundant group ($59 \pm 19\%$ of the total phytoplankton

586 cells counted), except at stations L5 and L6 where picoeukaryotes were dominant ($51 \pm 1\%$; Figure 9a-b). The

587 microeukaryotes were the least abundant group at all stations (average abundance across the sampling region of

588 $8 \pm 3\%$); however, due to their large biovolume, they contributed most to the biomass (average contribution to

589 biomass across the sampling region of $80 \pm 7\%$; Figure 9c). In the configuration used here, flow cytometry is best

590 suited for enumerating small cells ($<15\ \mu m$; Dubelaar and Jonker 2000), such that the larger microplankton present

591 at the time of sampling were likely underestimated via this technique. We thus take the phytoplankton net

592 collections as more representative of the microplankton community and colonial nanoplankton groups.

593

594 From the samples collected using the phytoplankton net (i.e., single or colonial cells $>55\ \mu m$), the dominant

595 phytoplankton species at LCIS was the prymnesiophyte, *P. antarctica* ($83 \pm 17\%$ of the total phytoplankton cells

596 counted), while the phytoplankton community at the other stations was dominated by diatoms (mainly *Corethron*

597 *pennatum, Chaetoceros spp.* (six species)*, Cylindrotheca closterium, Fragilariopsis ritscheri, Fragilariopsis*

598 *curta, Fragilariopsis kerguelensis, Fragilariopsis rhombica, Leptocylindrus mediterraneus, Odontella weisflogii,*

599 *Pseudo-nitzschia alanata* and several *Thalassiosira* spp., constituting $92 \pm 6\%$ of the total phytoplankton cells

600 counted; Figure 9d-e). At LCIS, the stations sampled earlier in the season tended to be dominated by *P. antarctica*

601 (e.g., station L3) while those sampled later hosted a more diatom-dominated community (e.g., station L8). In

602 addition, the resident diatoms at LCIS (mainly *F. ritscheri, O. weisflogii* and *Thalassiosira* spp.) were much larger

603 than the numerically dominant *P. antarctica* (by ~30- to 50-fold). For example, at station L8, the 32 diatom species

604 present (1603 cells L^{-1}) contributed 1.80 pg C L^{-1} (Leblanc et al. 2012) compared to 0.14 pg C L^{-1} resulting from

605 the 7812 cells L^{-1} of *P. antarctica* (Mathot et al. 2000). The LCIS stations with the highest relative abundance of

606 diatoms (e.g., station L8) were characterized by some of the highest rates of ρNO_3^- and greatest extent of NO_3^-

607 depletion. More broadly, the LCIS stations with the lowest SSTs and nutrient uptake rates (i.e., stations L1 and

608 L3) had the lowest phytoplankton counts, while those with the highest SSTs and nutrient uptake rates (i.e., station

609 L5) had the highest phytoplankton counts (Figure 9a and d; Table 1).

610

611
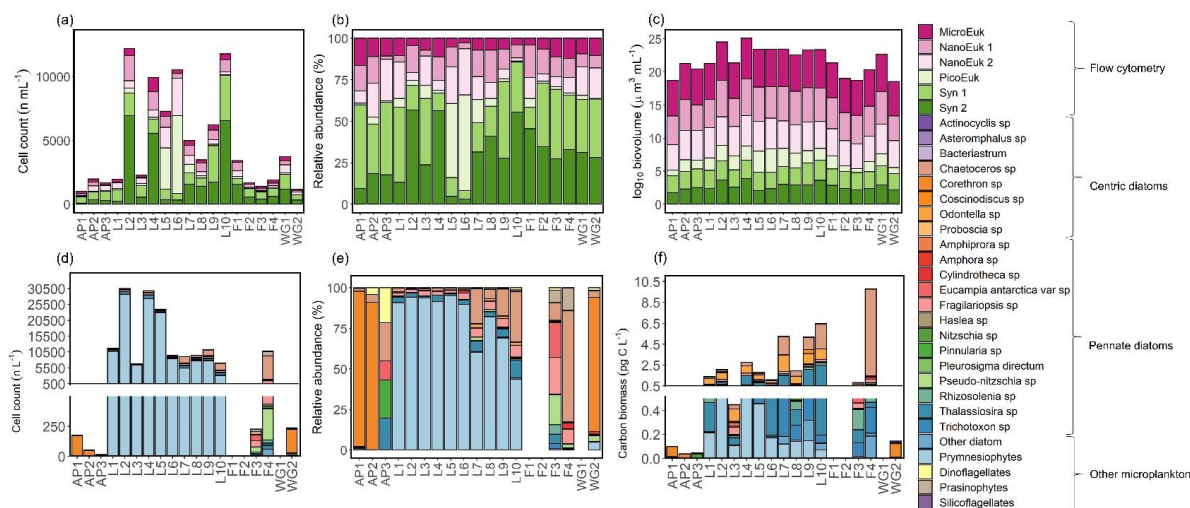
Figure 9. The (a, d) cell counts, (b, e) relative cell abundance, (c) log-transformed biovolume and (f) carbon biomass of all phytoplankton groups identified from the (a-c) surface flow cytometry samples and (d-f) phytoplankton net samples. Where there are no bars in panels (d), (e), and (f), no data are available. Carbon biomass estimates in panel (f) are only available for the prymnesiophyte, *P. antarctica,* and the diatom species.

Biogeosciences Discussions — Open Access — EGU

616

Table 1. Euphotic zone-averaged nutrient concentrations, nutrient depletions, and nutrient depletion ratios at each station occupied in the Weddell Sea in summer 2018/2019. Values shown are averages ± 1 SD (n ≥ 2). "-" indicates no available data.

Station position	Station	Sampling date	MLD (m)	Z_{eu} (m)	NH_4^+ (µM)	Urea-N (µM)	NO_3^- (µM)	NO_3^- depletion (µM)	$Si(OH)_4$ depletion (µM)	PO_4^{3-} depletion (µM)	$Si(OH)_4$:NO_3^- depletion	NO_3^-:PO_4^{3-} depletion
FIS Average	**FIS**		**82 ± 51**	**79 ± 28**	**0.1 ± 0.1**	**0.1 ± 0.1**	**25.0 ± 2.8**	**0.7 ± 1.4**	**1.6 ± 3.0**	**0.1 ± 0.1**	**2.0 ± 1.1**	**26.4 ± 19.8**
Fimbul	F1	01/01/19	135	100	0.0 ± 0.0	-	26.4 ± 0.5	0.2 ± 0.5	0.5 ± 1.6	0.0 ± 0.0	3.2 ± 3.9	-
Fimbul	F2	02/01/19	110	100	0.0 ± 0.0	-	26.5 ± 0.1	0.1 ± 0.1	0.0 ± 0.1	0.0 ± 0.0	0.5 ± 2.1	48.6 ± 11.5
Fimbul	F3	03/01/19	63	75	0.0 ± 0.0	0.0 ± 0.0	26.0 ± 0.3	0.7 ± 0.3	1.2 ± 0.5	0.0 ± 0.0	1.8 ± 0.6	18.8 ± 1.1
Fimbul	F4	20/02/19	20	40	0.2 ± 0.2	0.2 ± 0.1	20.2 ± 1.9	3.7 ± 2.0	8.7 ± 0.6	0.3 ± 0.1	2.3 ± 0.5	11.7 ± 0.6
AP Average	**AP**		**23 ± 8**	**45 ± 9**	**0.8 ± 0.2**	**0.3 ± 0.1**	**24.9 ± 0.6**	**2.5 ± 1.7**	**1.1 ± 0.8**	**0.1 ± 0.1**	**0.6 ± 0.2**	**19.8 ± 16.5**
Antarctic Peninsula	AP1	09/01/19	23	35	0.6 ± 0.1	0.2 ± 0.1	25.6 ± 1.4	2.6 ± 0.7	1.4 ± 0.4	0.2 ± 0.1	0.5 ± 0.4	14.1 ± 0.4
Antarctic Peninsula	AP2	09/01/19	30	50	0.7 ± 0.1	0.2 ± 0.1	25.9 ± 1.0	1.0 ± 1.1	0.8 ± 0.2	0.1 ± 0.0	0.8 ± 1.1	6.8 ± 1.1
Antarctic Peninsula	AP3	09/01/19	15	50	1.1 ± 0.0	0.3 ± 0.1	24.7 ± 0.3	3.2 ± 2.5	1.4 ± 1.5	0.1 ± 0.1	0.4 ± 1.4	38.4 ± 1.2
LCIS Average	**LCIS**		**14 ± 6**	**29 ± 9**	**0.7 ± 0.4**	**0.2 ± 0.1**	**16.4 ± 4.7**	**8.2 ± 4.9**	**8.1 ± 4.9**	**0.6 ± 0.3**	**1.0 ± 0.2**	**14.7 ± 2.9**
Larsen C	L1	22/01/19	8.5	33	1.3 ± 0.1	0.4 ± 0.1	21.8 ± 0.1	2.0 ± 0.1	2.3 ± 0.3	0.2 ± 0.1	1.2 ± 0.1	11.2 ± 0.3
Larsen C	L2	20/01/19	14	25	0.4 ± 0.3	0.2 ± 0.2	13.7 ± 5.0	8.6 ± 4.8	7.8 ± 4.7	0.6 ± 0.4	0.9 ± 0.8	15.2 ± 1.0
Larsen C	L3	11/01/19	7	50	0.9 ± 0.1	0.2 ± 0.1	23.1 ± 0.2	2.2 ± 0.1	1.3 ± 0.8	0.1 ± 0.1	0.6 ± 0.6	17.7 ± 0.3
Larsen C	L4	14/01/19	24	22	0.5 ± 0.5	0.1 ± 0.1	12.1 ± 2.5	12.8 ± 2.1	10.9 ± 2.2	0.9 ± 0.2	0.9 ± 0.3	13.9 ± 0.2
Larsen C	L5	15/01/19	10	25	0.1 ± 0.0	0.4 ± 0.2	12.0 ± 1.9	10.9 ± 2.3	9.6 ± 1.7	0.8 ± 0.1	0.9 ± 0.3	13.7 ± 0.2
Larsen C	L6	13/01/19	17.5	30	0.7 ± 0.5	0.2 ± 0.1	15.1 ± 2.1	8.4 ± 2.1	8.0 ± 1.9	0.4 ± 0.1	1.0 ± 0.3	20.4 ± 0.3
Larsen C	L7	22/01/19	8.5	25	1.0 ± 1.1	0.2 ± 0.1	14.7 ± 4.1	11.1 ± 1.8	13.5 ± 3.4	0.8 ± 0.2	1.2 ± 0.3	14.8 ± 0.3
Larsen C	L8	23/01/19	22.5	35	0.3 ± 0.0	0.2 ± 0.0	12.2 ± 2.2	12.9 ± 4.5	12.4 ± 3.2	0.8 ± 0.3	1.0 ± 0.4	16.0 ± 0.5
Larsen C	L9	19/01/19	12.5	20	0.5 ± 0.4	0.2 ± 0.1	20.2 ± 4.3	5.8 ± 3.3	6.6 ± 5.1	0.5 ± 0.3	1.1 ± 1.0	11.0 ± 0.9
Larsen C	L10	24/01/19	14	20	0.7 ± 0.3	0.2 ± 0.1	18.2 ± 5.4	8.7 ± 3.7	10.6 ± 4.9	0.7 ± 0.3	1.2 ± 0.6	13.0 ± 0.6
WG Average	**WG**		**20 ± 0**	**90 ± 14**	**0.2 ± 0.2**	**0.1 ± 0.1**	**28.8 ± 2.4**	**0.4 ± 0.3**	**2.0 ± 0.9**	**0.1 ± 0.0**	**5.6 ± 0.7**	**4.1 ± 0.6**
Weddell Gyre	WG1	14/02/19	20	100	0.2 ± 0.2	0.1 ± 0.1	26.7 ± 0.5	0.4 ± 0.3	2.3 ± 0.8	0.1 ± 0.0	5.1 ± 0.7	4.5 ± 0.7
Weddell Gyre	WG2	15/02/19	20	80	0.4 ± 0.1	0.1 ± 0.1	30.2 ± 0.8	0.3 ± 0.4	2.0 ± 1.0	0.1 ± 0.1	6.1 ± 1.3	3.7 ± 1.5

Biogeosciences
Discussions
Open Access
EGU

617

Table 2. Euphotic zone-integrated rates and averages at each station occupied in the Weddell Sea in summer 2018/2019. Values shown are averages $\pm$ 1 SD (n $\geq$ 2). "-" indicates no available data and the values shown in italics (i.e., purea) were estimated rather than measured (see text for details).

Station position	Station	[PON] (µM)	C:N ratio	NPP (mmol m⁻² d⁻¹)	ρNO_3^- (mmol m⁻² d⁻¹)	ρNH_4^+ (mmol m⁻² d⁻¹)	ρurea (mmol m⁻² d⁻¹)	$V NO_2^-$ (µmol m⁻² d⁻¹)	f-ratio (excluding urea)	f-ratio (including urea)
FIS Average	**FIS**	**0.8 ± 0.9**	**16.5 ± 8.8**	**27.5 ± 26.6**	**3.7 ± 1.0**	**0.8 ± 0.4**	**0.5 ± 0.4**	**0.3 ± 0.2**	**0.80 ± 0.10**	**0.73 ± 0.09**
Fimbul	F1	0.3 ± 0.2	21.6 ± 3.7	4.9 ± 0.0	3.8 ± 0.0	0.4 ± 0.0	*0.3 ± 0.0*	-	0.91	0.84
Fimbul	F2	0.2 ± 0.0	26.3 ± 12.6	20.8 ± 0.2	2.4 ± 0.0	0.8 ± 0.0	*0.07 ± 0.0*	-	0.75	0.70
Fimbul	F3	0.4 ± 0.2	8.8 ± 3.0	56.9 ± 0.6	4.8 ± 0.1	1.2 ± 0.0	*0.5 ± 0.0*	0.2 ± 0.0	0.80	0.74
Fimbul	F4	2.1 ± 0.6	9.4 ± 0.5	28.3 ± 0.4	3.9 ± 0.0	1.9 ± 0.0	*0.9 ± 0.0*	0.4 ± 0.0	0.68	0.63
AP Average	**AP**	**1.1 ± 0.3**	**8.3 ± 2.5**	**26.6 ± 33.5**	**3.4 ± 1.4**	**3.8 ± 2.0**	**0.5 ± 0.2**	**0.0 ± 0.1**	**0.52 ± 0.17**	**0.48 ± 0.16**
Antarctic Peninsula	AP1	1.3 ± 0.1	6.1 ± 1.4	3.1 ± 0.1	1.8 ± 0.1	2.6 ± 0.0	*0.4 ± 0.0*	0.0 ± 0.0	0.41	0.38
Antarctic Peninsula	AP2	0.8 ± 0.3	7.8 ± 2.7	11.8 ± 0.2	4.0 ± 0.2	2.1 ± 0.0	*0.4 ± 0.0*	0.0 ± 0.0	0.72	0.67
Antarctic Peninsula	AP3	1.3 ± 0.2	11.0 ± 2.1	65.0 ± 0.1	4.4 ± 0.0	5.8 ± 0.0	*0.8 ± 0.0*	0.1 ± 0.0	0.43	0.40
LCIS Average	**LCIS**	**2.4 ± 0.8**	**7.4 ± 1.9**	**28.6 ± 21.3**	**2.2 ± 1.1**	**2.6 ± 1.3**	**0.6 ± 0.3**	**0.5 ± 0.8**	**0.50 ± 0.09**	**0.47 ± 0.08**
Larsen C	L1	1.5 ± 0.3	10.0 ± 3.4	2.2 ± 0.1	1.5 ± 0.0	1.4 ± 0.0	*0.2 ± 0.0*	0.7 ± 0.0	0.52	0.50
Larsen C	L2	3.1 ± 0.5	6.3 ± 1.7	47.8 ± 0.5	1.5 ± 0.1	3.3 ± 0.0	*0.8 ± 0.0*	0.3 ± 0.0	0.54	0.51
Larsen C	L3	2.6 ± 0.8	5.8 ± 1.4	32.0 ± 0.1	2.5 ± 0.0	3.3 ± 0.0	*0.3 ± 0.0*	2.9 ± 0.0	0.42	0.41
Larsen C	L4	1.0 ± 0.2	8.0 ± 0.5	32.2 ± 1.0	1.9 ± 0.1	2.1 ± 0.0	*0.2 ± 0.0*	-	0.49	0.48
Larsen C	L5	3.1 ± 0.6	7.4 ± 1.9	61.0 ± 0.7	4.7 ± 0.0	3.1 ± 0.0	*0.9 ± 0.0*	0.1 ± 0.0	0.60	0.56
Larsen C	L6	2.4 ± 0.5	9.2 ± 5.3	25.9 ± 1.5	2.4 ± 0.1	2.2 ± 0.1	*0.7 ± 0.0*	0.4 ± 0.0	0.53	0.49
Larsen C	L7	1.5 ± 0.7	8.2 ± 1.1	55.9 ± 1.0	3.1 ± 0.0	3.8 ± 0.1	*1.1 ± 0.0*	0.0 ± 0.0	0.45	0.42
Larsen C	L8	3.3 ± 0.3	8.2 ± 1.3	17.3 ± 0.4	2.3 ± 0.0	4.8 ± 0.1	*0.9 ± 0.0*	0.4 ± 0.0	0.32	0.30
Larsen C	L9	2.9 ± 0.2	3.4 ± 4.1	9.7 ± 1.3	2.0 ± 0.1	1.2 ± 0.0	*0.6 ± 0.0*	0.5 ± 0.0	0.63	0.57
Larsen C	L10	2.7 ± 1.1	7.1 ± 0.4	1.8 ± 0.0	0.5 ± 0.0	0.6 ± 0.0	*0.2 ± 0.0*	0.1 ± 0.0	0.46	0.42
WG Average	**WG**	**0.7 ± 0.3**	**12.3 ± 1.8**	**31.6 ± 31.3**	**3.2 ± 0.1**	**2.0 ± 0.2**	**0.5 ± 0.1**	**9.0 ± 6.8**	**0.54 ± 0.10**	**0.48 ± 0.12**
Weddell Gyre	WG1	0.5 ± 0.2	13.6 ± 7.7	53.7 ± 0.2	3.3 ± 0.0	2.1 ± 0.0	*0.6 ± 0.0*	13.8 ± 0.2	0.47	0.39
Weddell Gyre	WG2	0.9 ± 0.3	11.0 ± 7.5	9.5 ± 0.4	3.1 ± 0.0	1.8 ± 0.0	*0.4 ± 0.0*	4.2 ± 0.0	0.61	0.56

618 **4. Discussion**

619 Across the Weddell Sea in summer 2019, the euphotic zone-integrated rates of NPP and N uptake were generally

620 lower at the OOZ stations than the CCSZ stations, with the highest depth-specific uptake rates observed in surface

621 waters at LCIS (Figure 6a-d; Table 2). The few studies that have previously measured summertime rates of NPP

622 and N uptake in the Weddell Sea reported similar results, with rates in the marginal ice zone (MIZ) and CCSZ

623 that were up to five-times higher than in the OOZ (El-Sayed and Taguchi 1981; Smith and Nelson 1990; Park et

624 al. 1999). The summertime CCSZ of the Weddell Sea can thus be broadly characterised as a highly productive

625 region with elevated biomass accumulation driven by increased water-column stratification and iron-replete

626 conditions, both the result of sea-ice melt (Semeneh et al. 1998; Lannuzel et al. 2008; Klunder et al. 2011).

627 However, we observed considerable variability in the biogeochemical rates measured within each region of the

628 Weddell Sea, particularly at LCIS; we examine the possible drivers of the inter- and intraregional differences

629 below.

630

631 **4.1. Drivers of NPP and N uptake in the Weddell Sea**

632 *Light and water column stability*: Surface waters throughout the study region were generally well stratified, with

633 MLDs ranging from 7 to 30 m, except at the early-summer FIS stations where the MLD ranged from 63 to 135 m

634 (Table 1). These deep MLDs coincided with elevated concentrations of sea-ice, while the shallowest MLDs

635 observed at LCIS occurred in relatively ice-free surface waters. Average euphotic zone rates of NPP and ρNO_3^-

636 generally varied with the depth of the mixed layer and Z_{eu} at all stations – they were highest (lowest) at the stations

637 where Z_{eu} was shallowest (deepest) (Figure 10a-b), implicating light as a major control on NPP and ρNO_3^-. At

638 LCIS, however, the euphotic zone was shallow at all stations (<50 m, average Z_{eu} of 28.5 ± 9 m), yet NPP and

639 ρNO_3^- varied by over an order of magnitude (Table 2). We observed a positive relationship between the LCIS

640 rates and SST, with NPP and ρNO_3^- increasing at higher SSTs, the latter indicative of increased water column

641 stratification (Figure 10d; see below).

642

643 Throughout the region, the average euphotic zone rates of ρNH_4^+ and $\rho urea$ also varied with Z_{eu} (Figure 10c),

644 suggesting that these processes were light dependent too. This is unexpected, as the energy requirement associated

645 with NH_4^+ and urea assimilation is low (El-Sayed and Taguchi 1981; Dortch 1990; Jacques 1991; Goeyens et al.

646 1995; Priddle et al. 1998). The stations with the deepest Z_{eu} were also characterized by low concentrations of

647 regenerated N (Figures 3a-b and 10c), leading us to conclude that ρNH_4^+ and $\rho urea$ were predominantly

648 constrained by the availability of regenerated N rather than by light. This conclusion is supported by the observed

649 increase in ρNH_4^+ and $\rho urea$ towards the base of the euphotic zone at stations with elevated regenerated N

650 concentrations (e.g., station L8; Figures 6c-d, g-h, and k-l, and 10c).

651

652 The lowest regenerated N concentrations occurred at the stations with the lowest rates of NPP and ρNO_3^-, and the

653 highest NO_3^- concentrations (e.g., station F1). This is probably because NH_4^+ and urea tend to accumulate only

654 when biomass (and productivity) is sufficiently high to support elevated rates of heterotrophic activity (Semeneh

655 et al. 1998). At the stations with low POC and PON concentrations, remineralisation rates were likely also low,

656 limiting the flux of NH_4^+ and urea and driving low rates of ρNH_4^+ and $\rho urea$. At the stations where NH_4^+ and urea

657 concentrations were elevated, rates of ρNH_4^+ and $\rho urea$ increased with depth, along with a decrease in NPP and

658 ρNO_3^- (e.g., station L8). These observations further demonstrate the control of light on NPP and ρNO_3^-, and

659 substrate availability on ρNH_4^+ and ρurea. That said, it is unlikely that the variability in NPP and N uptake among

660 the stations was driven by light and nutrient availability alone, and we hypothesize that hydrography, iron

661 availability, and phytoplankton community composition also played a role.

662
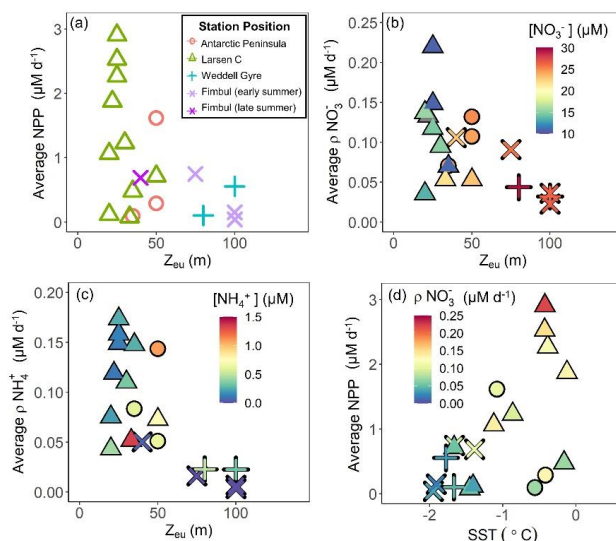
663

Figure 10. Euphotic zone-averaged rates of (a) NPP, (b) ρNO_3^- and (c) ρNH_4^+ versus Z_{eu}, and (d) NPP versus SST
665 at each station. The symbols in panels (b) and (c) are coloured by nutrient concentration and in panel (d), by ρNO_3^-
666

667 At LCIS, the stations closest to the ice shelf were characterised by low SSTs and low rates of NPP and N uptake

668 (stations L1 and L3; Figures 1 and 11a; Table 2). The low SSTs can be attributed either to the formation of sea-

669 ice or to the upwelling of WW along the ice shelf. Sea-ice formation, in addition to decreasing SST, also increases

670 the salinity of ASW due to brine rejection (Brennecke 1921; Mosby 1934; Gill 1973). While the salinity of ASW

671 at the low-SST stations was indeed elevated, the oxygen concentrations were relatively low (≤ 300 µM, which is

672 below saturation; Figure 11c and d). In surface waters and sea-ice, oxygen is typically saturated as it rapidly

673 equilibrates with the atmosphere (Gleitz et al. 1995). Sea-ice formation should not, therefore, drive a notable

674 change in the oxygen content of ASW. The low oxygen concentrations at stations L1 and L3 were contiguous

675 with those in the underlying WW (Figure 11d), leading us to conclude that the cool, saline waters along the ice-

676 shelf front indicate recent upwelling of WW. Such upwelling could temporarily inhibit productivity by decreasing

677 the stability of the water column, thereby mixing phytoplankton below the euphotic zone. This mechanism can

678 explain the low uptake rates and weak nutrient depletions observed at the low-SST stations.

679

680 Relatively cold, saline surface waters have previously been observed at the ice-edge off Larsen A and B Ice

681 Shelves and shown to hinder NPP (Cape et al. 2014). Here, the dense surface waters were surmised to result either

682 from offshore wind stress at the inshore region that induced localised mixing, or from the advection of surface

683 waters offshore by coastal upwelling. Both mechanisms would decrease water column stability, and by extension,

684 productivity. Cape et al. (2014) observed an increase in NPP with distance from the coast at Larsen A and B, a

685 trend that we did not observe, likely because of the proximity of our LCIS stations to the ice shelf (within 75 km

686 for all stations). Instead, our rates of NPP and N uptake were positively coupled with SST at the ice-edge (Figure

687 10d). We propose that surface SST at LCIS can be used as an indicator of water-mass age, with cooler SSTs

688 indicating newly-upwelled WW and warmer SSTs designating older surface waters that have had time to absorb

689 heat from the atmosphere. The higher rates of NPP and N uptake in the warm surface waters occur because

690 phytoplankton have experienced favourable growing conditions for an extended period, resulting in the

691 accumulation of biomass. By contrast, persistent localised upwelling along LCIS inhibits productivity in the

692 adjacent surface waters, with implications for the spatial distribution of biomass and organic carbon export.

693
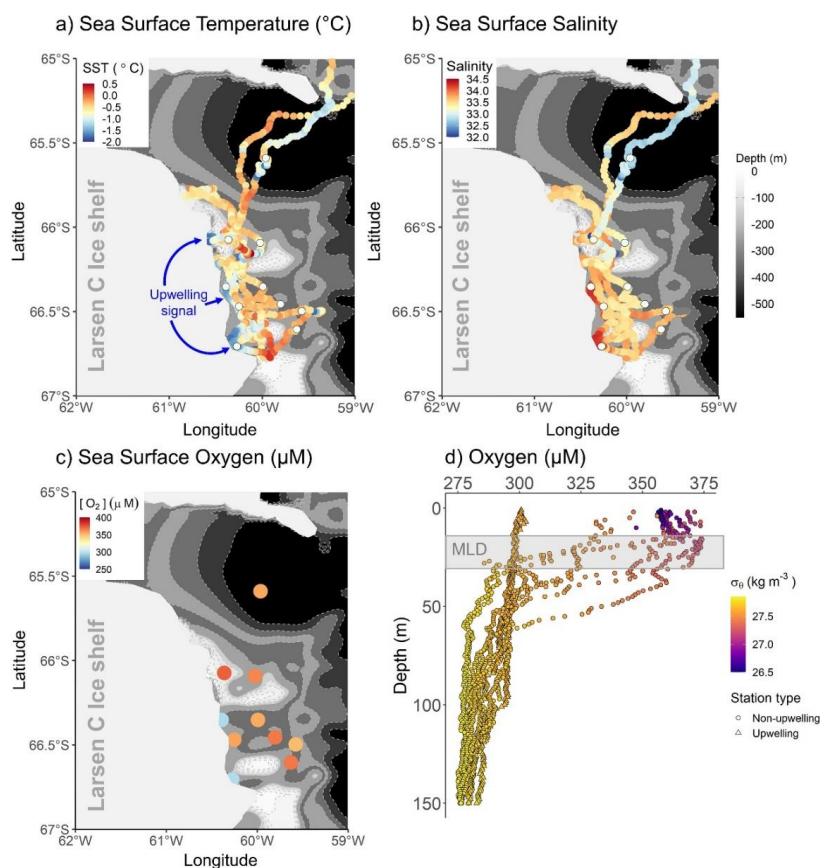
695 **Figure 11.** Maps of (a) SST, (b) sea surface salinity, and (c) surface oxygen concentrations, and (d) depth profiles
696 of oxygen concentrations in the region of LCIS at the time of sampling. SST and salinity data were acquired from
697 the underway (~7 m inflow) ferrybox, while the oxygen concentrations were measured via the oxygen sensor on
698 the CTD profiler, calibrated against discrete seawater samples measured for dissolved oxygen by Winkler titration
699 (Carpenter 1965; Grasshoff et al. 1983; Hutchinson et al. 2020)(Carpenter 1965; Grasshoff, Kremling, and
700 Ehrhard 1983)(Carpenter 1965; Grasshoff, Kremling, and Ehrhard 1983)(Carpenter 1965; Grasshoff, Kremling,
701 and Ehrhard 1983)(Carpenter 1965; Grasshoff, Kremling, and Ehrhard 1983). The symbols in panel (d) are
702 coloured by potential density (σ_θ), with the circles indicating the non-upwelling stations and the triangles the
703 upwelling stations. The grey box in panel (d) indicates the average mixed layer depth (MLD) across the stations
704 at LCIS. The bathymetry data in panels (a-c) were taken from ETOPO1 (NOAA National Geophysical Data Center
705 2009).

706   *Nutrient and iron conditions in Weddell Sea surface waters*: Across our sampling region, ASW was depleted in

707   NO_3^-, $Si(OH)_4$ and PO_4^{3-} relative to the underlying WW, with the greatest nutrient depletion occurring at LCIS

708   and at FIS in late summer (Figure 4a-c). Under iron-replete conditions, diatoms consume Si:N:P in an approximate

709   ratio of 1:1:0.07 (Ragueneau et al. 2000; Hutchins and Bruland 1998; Takeda 1998; Mosseri et al. 2008), while

710   under iron-limitation, they increase their uptake of Si and decrease that of P relative to N, consuming nutrients in

711   a ratio of ≥2:1:0.09 (Arrigo et al. 1999; Finkel et al. 2006; Green and Sambrotto 2006; Weber and Deutsch 2010;

712   Martiny et al. 2013; Mosseri et al. 2008), with Si:N uptake ratios as high as 8:1 occurring when iron is very low

713   (Franck et al. 2000; Brzezinski et al. 2003). The Si:N:P depletion ratios (more correctly, $Si(OH)_4$:NO_3^-:PO_4^{3-}

714   depletion ratios) estimated in our study suggest that the AP and LCIS stations were characterised by iron-replete

715   conditions (ratio of 0.9:1:0.06) while the phytoplankton community at the FIS and WG stations experienced iron

716   limitation (ratios of 3.6:1:0.15; Figures 4d and 4e; Table 1).

718   High iron concentrations have previously been measured in surface waters in the CCSZ and northern Weddell Sea

719   (7 nM; Lannuzel et al. 2008; De Jong et al. 2012). Iron is supplied to the mixed layer in these regions via sea-ice

720   melt, ice shelf melt, continental runoff, vertical and lateral advection, and resuspension of continental shelf

721   sediments (Lannuzel et al. 2008; De Jong et al. 2012; Klunder et al. 2014). In contrast, the central WG is iron

722   limited as iron is supplied to surface waters mainly by wind-induced vertical mixing (Hoppema et al. 2015).

723   During our sampling, sea-ice concentrations were high at the WG stations, which would have dampened the effect

724   of wind stress on surface waters and thus hindered vertical mixing. At FIS in early summer, iron is expected to be

725   replete as phytoplankton will not have had sufficient time to exhaust the surface reservoir. Here, the sea-ice

726   concentrations were elevated, and the mixed layers were deep such that light, rather than iron, likely limited

727   phytoplankton growth. Light-limited diatoms have been observed to consume Si:N:P in a ratio similar to that

728   reported under conditions of iron depletion (Brzezinski 1985). By late summer at FIS, the sea-ice had completely

729   melted, which should have further alleviated iron limitation, yet the $Si(OH)_4$:NO_3^- depletion ratios were

730   characteristic of iron-deplete diatoms (average of 2.3 ± 0.5). These apparently high Si:N depletion ratios may be

731   due to our not accounting for regenerated N uptake. At FIS in late summer, NH_4^+ supported 32% of N uptake;

732   accounting for this N source decreases the Si:N depletion ratio to 1.4:1, which is closer to that expected for iron-

733   replete diatoms. While some diatom growth was likely also supported by urea, which would further decrease the

734   Si:N depletion ratio, it is nonetheless plausible that the diatoms at F4 were beginning to experience iron-limitation

735   as the station was sampled late in the season.

737   Accounting for regenerated N uptake greatly alters the Si:N depletion ratios, particularly at LCIS, and provides

738   insights into the dominant phytoplankton groups that were active in the mixed layer, both prior to and at the time

739   of sampling. From the Si:NO_3^- depletion ratio at LCIS, we infer that *P. antarctica* predominantly consumed

740   regenerated sources of N. Our reasoning relies on that fact that under favourable nutrient and light conditions,

741   diatoms will rely near-exclusively on NO_3^- (Lomas and Glibert 1999), such that the average Si:NO_3^- depletion

742   ratio at LCIS of 1.0 ± 0.2 can be attributed entirely to this phytoplankton group. When total N uptake is considered,

743   the Si:N depletion ratios decrease to 0.3 ± 0.1, indicating the consumption of three-times more N than $Si(OH)_4$,

744   which we attribute to regenerated N uptake by *P. antarctica*. Indeed, this phytoplankton group is known to

745   preferentially consume NH_4^+ when it is available due to the lower energy (El-Sayed and Taguchi 1981; Dortch

746   1990; Jacques 1991; Goeyens et al. 1995; Priddle et al. 1998) and iron requirements (Stefels and Van Leeuwe

747   1998) associated with NH_4^+ assimilation. By contrast, diatoms are NO_3^- specialists that can outcompete other

748   phytoplankton for this N source (Malone 1980; Fawcett and Ward 2011). They have even been observed to

749   consume NO_3^- under iron-deplete conditions, which is possible because of their low iron requirement relative to

750   that of other phytoplankton groups (Marchetti and Maldonado 2016; Marchetti and Cassar 2009).

751

752   We can also use the NO_3^-:PO_4^{3-} depletion ratios to better understand the iron conditions and the relative importance

753   of *P. antarctica* versus diatoms in generating the observed nutrient depletion ratios. *P. antarctica* are known to

754   consume NO_3^- and PO_4^{3-} in a ratio of ~20:1, while for iron-replete diatoms, this ratio is <14:1 (Arrigo et al. 1999;

755   Smith and Asper 2001; Garcia et al. 2018). At LCIS, the NO_3^-:PO_4^{3-} depletion ratio averaged 14.7 ± 2.9, consistent

756   with a dominant role for iron-replete diatoms. However, variability in the NO_3^-:PO_4^{3-} depletion ratios was

757   observed among the LCIS stations (with ratios ranging from 11 to 20), which we attribute to local variations in

758   phytoplankton community composition. At stations where large diatoms were dominant (e.g., L10, where diatoms

759   contributed 6.47 pg C L^{-1} to biomass while *P. antarctica* only contributed 0.07 pg C L^{-1}; Leblanc et al. 2012;

760   Mathot et al. 2000), the NO_3^-:PO_4^{3-} depletion ratios were low (13.0 ± 0.6). In contrast, at the stations where *P.*

761   *antarctica* were numerically dominant (e.g., L6; where *P. antarctica* constituted 90% of the phytoplankton

762   population) and contributed more to biomass (0.17 pg C L^{-1}), elevated NO_3^-:PO_4^{3-} depletion ratios were measured

763   (20.4 ± 0.3; Figure 9d-f; Table 1). Furthermore, high rates of NH_4^+ uptake were measured at LCIS, equivalent to

764   and at times greater than the coincident NO_3^- uptake rates. *P. antarctica* has been observed to preferentially

765   consume NH_4^+, while diatoms will consume NO_3^- if iron is available (Probyn and Painting 1985; Lomas and

766   Glibert 1999; Glibert et al. 2016). The relative contribution of diatoms versus *P. antarctica* to biomass thus

767   appears to control the nutrient depletion ratios on a variety of scales across the Weddell Sea.

768

769   *Drivers of phytoplankton community composition*: Phytoplankton community composition and the variations

770   therein have implications for the biological pump, both directly (diatoms sink more rapidly than smaller and/or

771   non-ballasted phytoplankton; Treguer and Jacques 1992; De Baar et al. 2005; Boyd et al. 2007) and indirectly

772   (NO_3^- consumption is quantitatively related to carbon export; Dugdale and Goering 1967; Eppley and Peterson

773   1979). Above, we have discussed the biogeochemical evidence for the dominance of one phytoplankton group

774   over another in driving productivity and nutrient consumption. Below, we discuss the processes that may have

775   resulted in the dominance of *P. antarctica* over diatoms at LCIS, and vice versa at the other Weddell Sea stations.

776

777   At LCIS, a coastal sensible heat polynya persisted throughout the sampling period. The opening of such polynyas

778   along the eastern AP is linked to the occurrence of warm, föhn winds that originate over the continent and blow

779   over the AP, influencing the coastal north-western Weddell Sea (Cape et al. 2014). Föhn winds drive the offshore

780   movement of sea-ice, which initiates the opening of polynyas that persist because the winds are warm, thus

781   hindering the formation of new sea-ice (Cape et al. 2014). The development of coastal sensible heat polynyas

782   results in relatively deep mixed layers and a weakly stratified water column. The polynya at LCIS opened in late

783   November, approximately two months prior to our sampling. At this time (i.e., the beginning of the growing

784   season), motile *P. antarctica* cells likely dominated the phytoplankton community as *P. antarctica* are low-light

785   specialists compared to other Antarctic phytoplankton (Goffart et al. 2000; Delmont et al. 2014). This notion is

786   supported by the low phytoplankton cell counts (for both flow cytometry and net samples) and high relative
787   abundance of *P. antarctica* compared to diatoms at the stations along the ice shelf where WW had recently
788   upwelled (e.g., L3; Figure 9a, d and e). As the mixed layer shoaled and light limitation was alleviated, a diatom
789   bloom would have been initiated and *P. antarctica* colony formation would have occurred (Schoemann et al.
790   2005). Indeed, the presence of *P. antarctica* (as colonies) and diatoms (as chains) at the time of our sampling in
791   January is evidence that the water column was well stratified (Goffart et al. 2000). As the season progressed,
792   diatoms would have outcompeted *P. antarctica* and come to dominate the phytoplankton community. At the
793   stations sampled later in the season (e.g., L10; Figure 9e), the relative abundance of diatoms versus *P. antarctica*
794   was greater than at the stations sampled two weeks earlier (e.g., L5; Figure 9e). Diatoms have a lower iron and
795   higher light requirement than *P. antarctica* and thus tend to thrive once the *P. antarctica* bloom is over, when the
796   water column has stratified and they can utilize the lower concentrations of residual iron (Strzepek et al. 2011).
797   That said, iron is likely perennially high at LCIS as it is near-continuously supplied to surface waters in summer
798   by sea-ice melt and upwelling of WW along the ice shelf (Klunder et al. 2014). The elevated iron concentrations
799   would allow the diatoms to grow rapidly on the available NO_3^- once the mixed layer had shoaled enough to
800   alleviate light limitation.
801
802   Throughout the rest of the Weddell Sea, diatoms dominated the phytoplankton community. Here, we hypothesize
803   that at the beginning of the growing season, melting sea-ice alleviated light- and, to a lesser extent, iron limitation,
804   providing favourable conditions for diatom growth. At the same time, the generally lower iron concentrations
805   characteristic of open Weddell Sea waters may have selected against *P. antarctica*. Previous studies conducted in
806   the Ross Sea observed large diatom blooms associated with the receding ice-edge and concluded that bloom
807   formation was favoured by the rapid stabilization of the water column from meltwater inputs (Goffart et al. 2000;
808   Sedwick et al. 2000). Regions of the Weddell Sea that undergo rapid stratification due to sea-ice melt will likely
809   also experience large diatom blooms. We thus conclude that the dominance of diatoms over *P. antarctica* at the
810   non-LCIS stations was influenced by local hydrodynamic processes that induce water column stability and allow
811   access to sufficient light (e.g., in areas of recent sea-ice melt). By contrast, *P. antarctica* dominates under
812   conditions of low light, such as the deep mixed layers that initially characterize coastal polynyas. Eventually,
813   diatoms will succeed *P. antarctica* in these polynyas once conditions become favourable for their growth.
814

4.2. Carbon export potential across the Weddell Sea

816   Previous f-ratio estimates for the summertime Weddell Sea range from 0.18 to 0.83 (Koike et al. 1986; Rönner et
817   al. 1983; Nelson et al. 1987; Smith and Nelson 1990; Goeyens 1991; Goeyens et al. 1995). Using equations 4a
818   and 4b, we calculate euphotic zone-integrated f-ratios that range from 0.32 to 0.91 (excluding urea uptake) and
819   0.30 to 0.84 (including urea uptake). The lowest f-ratios were observed at LCIS (f-ratio$_{(excluding\ urea)}$ = 0.50 ± 0.09
820   and f-ratio$_{(including\ urea)}$ = 0.47 ± 0.08) and the highest at FIS (f-ratio$_{(excluding\ urea)}$ = 0.78 ± 0.1 and f-ratio$_{(including\ urea)}$ =
821   0.73 ± 0.09) (Figure 8; Table 2). We note that urea uptake may have been stimulated at the stations where it was
822   measured given the quantity of ^{15}N-urea added (0.1 μM) relative to the ambient urea concentrations (average of
823   0.2 ± 0.1 μM; Figure S2; section S3 in the Supplemental Information); if so, regenerated production could be
824   overestimated at all stations since we applied the average measured contribution of urea-to-total-N uptake (8 ±
825   6%) to the stations at which ρurea was not measured (equation 7). The f-ratio estimates excluding and including

826   urea uptake thus represent an upper and lower bound on the fraction of potentially exportable carbon. That said,

827   accounting for urea uptake decreased the average f-ratio from 0.57 ± 0.15 to 0.52 ± 0.14 which is minor (Figure

828   8; Table 2).

829

830   Estimates of the f-ratio and carbon export potential can be further complicated by euphotic zone nitrification,

831   which supplies regenerated rather than new NO_3^- to the euphotic zone. Failing to account for this regenerated N

832   flux leads to an overestimation of carbon export potential (Yool et al. 2007; Mdutyana et al. 2020). At all the

833   stations sampled, the euphotic zone rates of $V_{NO_2^-}$ were low (undetectable to 9.5 nM d^{-1}; Figure 7b) and correcting

834   the f-ratio for euphotic zone nitrification (equation 4) had a minimal effect on our estimates (average decrease of

835    $2 \pm 6\%$). The largest decrease was observed at WG1 where the highest euphotic zone-integrated rates of $V_{NO_2^-}$

836   were measured (f-ratio$_{(excluding\ urea)}$ decreased from 0.6 to 0.47 and f-ratio$_{(including\ urea)}$ decreased from 0.49 to 0.39;

837   Table 2).

838

839   The low rates of euphotic zone nitrification are consistent with the previous (limited) data available for the

840   summertime OOZ and CCSZ of the Southern Ocean. For example, Mdutyana et al. (2020) measured euphotic

841   zone rates of $V_{NO_2^-}$ and NH_4^+ oxidation in summer at FIS and in the Antarctic Zone just north of the WG (56°S

842   0°E) that were below detection. Summertime studies of euphotic zone NH_4^+ oxidation in the Ross and Scotia Seas

843   reported similarly low rates of 6-8.9 nM d^{-1} and 0.4-5.8 nM d^{-1}, respectively (Olson 1981). We conclude that, as

844   expected, the high-light and generally low-NH_4^+ conditions of the summertime Weddell Sea inhibited euphotic

845   zone nitrification (Horrigan 1981; Olson 1981; Guerrero and Jones 1996; Merbt et al. 2012; Qin et al. 2014), and

846   that the slow growing nitrifiers were likely also outcompeted by phytoplankton for any available NH_4^+ (Ward

847   1985; 2005; Smith et al. 2014; Zakem et al. 2018). Classifying NO_3^- uptake as new production and equating it to

848   carbon export potential thus seems reasonable for the summertime Weddell Sea.

849

850   Although the highest f-ratios were estimated for the FIS stations, the highest rates of ρNO_3^- were observed at LCIS

851   and along the AP (Figure 8; Table 2). FIS was thus characterised by the highest carbon export potential relative

852   to NPP, while the N cycle data imply that the absolute carbon export flux was highest at LCIS and the AP. The

853   maximum extent of nutrient depletion was also observed at LCIS (NO_3^- depletion of 57-428 mmol m^{-2} and PO_4^{3-}

854   depletion of 5.8-18.7 mmol m^{-2}). Assuming Redfield C:N and C:P stoichiometry of 6.63:1 and 106:1, respectively,

855   the seasonal NO_3^- depletion equates to a carbon export flux of 0.4-2.8 mol C m^{-2} and the PO_4^{3-} depletion to 0.6-

856   2.0 mol C m^{-2}. Alternately, multiplying ρNO_3^- by the length of time that the coastal polynya had been open (30

857   November until the date of sampling; Table 1) yields an estimate for net seasonal NO_3^- uptake of 59-428 mmol

858   m^{-2} and carbon export flux of 0.4-2.8 mol C m^{-2} at LCIS, remarkably similar to the estimates derived from seasonal

859   NO_3^- depletion. Our estimates are, however, lower than those previously measured in the CCSZ and MIZ of the

860   Weddell Sea (e.g., estimates for January/February range from 2.4-4.9 mol C m^{-2}; Rönner et al. 1983; Hoppema et

861   al. 2000; 2007). Given the high-light and nutrient- and iron-replete conditions at LCIS, one might thus have

862   expected higher f-ratios and carbon export potential (i.e., NO_3^- depletion), raising the question of the possible

863   limitations thereon.

864

865   Throughout the Weddell Sea, NH_4^+ and urea uptake were coupled with substrate availability, while NO_3^- uptake

866   was not. Instead, NO_3^- uptake appeared to vary as a function of the ambient NH_4^+ concentration (Figure 12a). At

867   LCIS where NH_4^+ was elevated throughout the mixed layer at all stations, NO_3^- depletion, and therefore NO_3^-

868   uptake, decreased with increasing NH_4^+ (Figure 12b), which we attribute to NH_4^+ inhibition of NO_3^- uptake

869   (Goeyens et al. 1995). By contrast, at the other stations, NO_3^- depletion and ambient NH_4^+ concentration showed

870   a positive relationship, consistent with NO_3^--fuelled phytoplankton growth being followed by intense

871   remineralization and grazing, both of which can yield elevated NH_4^+ (Rönner et al. 1983; El-Sayed 1984; Semeneh

872   et al. 1998).

873
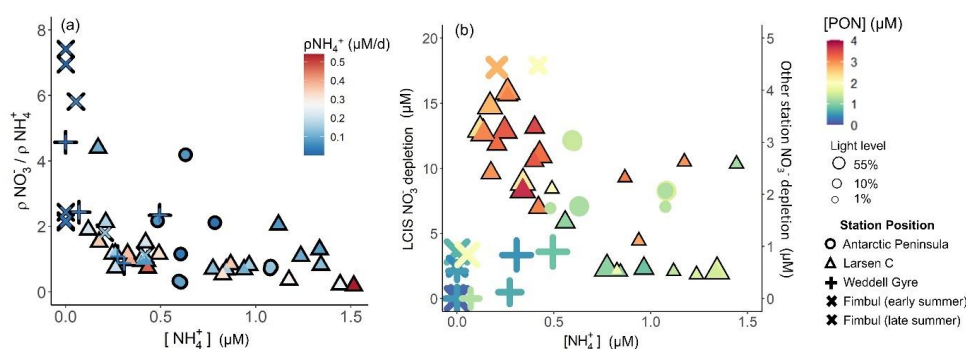
874

Figure 12. (a) NO_3^- uptake normalised to NH_4^+ uptake versus NH_4^+ concentration and b) NO_3^- depletion versus
NH_4^+ concentration. The symbols in panel (a) are coloured by NH_4^+ uptake rate and in panel (b) by PON
concentration. The symbol size in panel (b) represents the light level at which the samples were incubated. In
panel (b), NO_3^- depletion at LCIS corresponds with the primary y-axis and NO_3^- depletion at all other stations
corresponds with the secondary y-axis.

880

881   Previous studies conducted in MIZ and CCSZ of the Weddell Sea have shown that NH_4^+ concentrations ≥0.5 µM

882   can inhibit NO_3^- uptake, particularly by diatoms, resulting in phytoplankton preferentially consuming NH_4^+ over

883   NO_3^-. Goeyens et al. (1995) observed a Weddell Sea phytoplankton community dominated by diatoms prior to

884   NH_4^+ accumulation, but once surface waters became enriched in NH_4^+, diatom dominance ceased. The authors

885   concluded that diatom blooms were unable to develop despite the elevated NO_3^- because of the inhibitory effect

886   of NH_4^+, while non-siliceous phytoplankton species flourished because their preferred N source is NH_4^+. In our

887   study, although NH_4^+ inhibition of ρNO_3^- apparently occurred at LCIS, the rates of ρNO_3^- were on average as high

888   as ρNH_4^+ and were never zero (Table 2) – in other words, the high ambient NH_4^+ did not prevent NO_3^- uptake

889   even though it appears to have slowed it. We propose that the mixed community of diatoms and *P. antarctica*

890   present at the time of our sampling meant that diatoms were able to consume NO_3^- while *P. antarctica* consumed

891   the NH_4^+, preventing this reduced N form from accumulating to fully inhibitory concentrations. While the reliance

892   of *P. antarctica* on NH_4^+ over NO_3^- represents a missed opportunity for carbon export given that *P. antarctica* are

893   known to fix up to 50% more carbon than diatoms per mole of PO_4^{3-} consumed (Arrigo et al. 1999), that the

894   diatoms were able to proliferate in the face of elevated NH_4^+ may have partly compensated for this. Earlier in the

895   season when NH_4^+ concentrations were negligible, it is likely that the f-ratios at LCIS were >0.5 and comparable

896   to those at FIS, as observed at Larsen A and B in early summer (Goeyens et al. 1995; Cape et al. 2014). We

897   conclude that elevated NH_4^+ may have weakened carbon export potential at LCIS in January/February 2019

898 through its effect on whole-community NO_3^- uptake. Carbon export may have been further inhibited later in the
899 season as NH_4^+ concentrations continued to increase following remineralisation of the phytoplankton bloom,
900 coupled with the seasonal decrease in daylight that is expected to shift the phytoplankton community to
901 proportionally higher NH_4^+ dependence (Glibert et al. 2016).
902

903 **4.3. Broader biogeochemical implications at LCIS**
904 LCIS is a region of deep-water formation, such that the biogeochemical properties of ASW influence those of
905 MWDW and the bottom waters. Over the summer growing season, there was significant net depletion of nutrients
906 from ASW. These nutrients were converted to organic matter (OM), which was then either consumed by
907 zooplankton or exported out of the euphotic zone and decomposed by heterotrophic bacteria on the shelf and in
908 the overlying waters. The on-shelf remineralisation of OM acts to increase the CO_2 and nutrient reservoir of WW
909 and shelf waters (ISW and HSSW; both precursors of CDW). Some portion of this CO_2 is effluxed to the
910 atmosphere when WW upwells along the ice shelf front, while the rest will be mixed into MWDW and eventually
911 transferred to the bottom waters where it will be stored for hundreds of years (Ito et al. 2010). Biological activity
912 and nutrient drawdown at LCIS, and the limitations thereon, thus affect the CO_2 and nutrient content of the bottom
913 waters. The $Si(OH)_4$:NO_3^-:PO_4^{3-} ratio at depth at LCIS (average of 2:1:14 below 150 m) implicates diatoms as the
914 main biological driver of the nutrient conditions in MWDW, and by extension the bottom waters, throughout the
915 Weddell Sea. Although the dominance of *P. antarctica* in early and mid-summer does not appear to affect the
916 nutrient properties of MWDW, it likely influences its CO_2 content. *P. antarctica* consume approximately twice
917 as much carbon per PO_4^{3-} as diatoms, and the colonial forms have been observed to rapidly sink out of the water
918 column, thereby transporting large quantities of carbon to depth (Arrigo et al. 2000; Ditullio et al. 2000). The
919 dominance of *P. antarctica* at LCIS may thus be important for carbon storage in MWDW and the bottom waters.
920

921 As SSTs rise and sea-ice melts, a shift from *P. antarctica*- to diatom-dominated phytoplankton blooms is expected
922 because diatoms flourish under conditions of high light and water column stratification (i.e., in areas of recent
923 sea-ice melt) (Boyd and Doney 2002; Arrigo and van Dijken 2003; Petrou et al. 2016; Ferreira et al. 2020). Given
924 the anomalously high carbon-to-nutrient content of *P. antarctica*, such a shift may negatively affect the export
925 and storage of carbon in MWDW and the bottom waters. However, rising SSTs will also lead to increased glacial
926 and ice shelf melt, further stratifying the adjacent water column and increasing the iron supply (Petrou et al. 2016).
927 It is projected that these conditions will yield blooms of heavily-silicified diatom species (Deppeler and Davidson
928 2017) that are known to sink rapidly out of the mixed layer or, if consumed, their frustules are expected to survive
929 the gut passages of copepods, resulting in increased carbon export (Assmy et al. 2013). However, this increase is
930 unlikely to be two-fold that presently contributed by diatoms, and therefore not as high as the carbon export
931 potential associated with colonial *P. antarctica*. In net, the expected floristic shift may lead to decreased carbon
932 export at the ice shelves, in turn decreasing the carbon content of the MWDW formed at LCIS. Further
933 investigation of the drivers of phytoplankton community composition is required to validate this notion,
934 particularly with regards to the response of Antarctic phytoplankton to warming, as well as how changes in the
935 surface ecosystem are transferred to and reflected in the biogeochemistry of bottom waters.
936
937

5. Conclusions

In this study, we investigated the summertime productivity of understudied regions of the Weddell Sea, including LCIS, and the potential importance of different phytoplankton groups for biomass production, nutrient consumption, and carbon export. Our data show that mixed-layer nutrient depletion ratios were determined by the dominant phytoplankton group. The lowest Si:N and highest N:P depletion ratios were observed at LCIS (consistent with *P. antarctica* dominance), while the highest Si:N and lowest N:P depletion ratios were estimated at FIS and in the WG (consistent with diatom dominance). The variability in phytoplankton community composition appears to have been largely driven by mechanisms controlling water column stratification. *P. antarctica* are low-light specialists and proliferated at LCIS due to the deep mixed layers that occurred early in the season, while diatoms dominated at stations where the upper water column was more stratified and the mixed layer was shallow, induced by sea-ice melt. Not only does the observed relationship between phytoplankton community composition and the nutrient depletion ratios have implications for the stoichiometry of the deep-water nutrient reservoir, but it likely also has consequences for carbon export and storage.

Although the waters adjacent to LCIS were characterized by the highest NO_3^- uptake rates, the lowest f-ratios were also observed here. We attribute these low f-ratios to some degree of NH_4^+ inhibition of NO_3^- uptake, which translates to a missed opportunity for carbon export (Cochlan and Bronk 2003) and potentially, long-term storage in bottom waters, particularly since neither NO_3^- nor iron appeared to be limiting at the time of our sampling. Additional investigation is required to ascertain the persistence of NH_4^+ inhibition in the Antarctic CCSZ, particularly in regions of deep-water formation (e.g., at Filchner-Ronne Ice Shelf). Furthermore, given the prediction that the Weddell Sea's upper water column will become more stratified with climate change (Pörtner et al. 2014; Sallée et al. 2013; Stammerjohn et al. 2012), it is essential that we improve our understanding of the physical and chemical drivers of phytoplankton community composition and functioning if we are to better predict changes to carbon drawdown via the biological pump.

6. Figure and table captions

Figure 1. Maps of the Weddell Sea, Larsen C Ice Shelf (LCIS; insert a) and Fimbul Ice Shelf (FIS; insert b) showing the position of the stations where rate experiments were conducted during the Weddell Sea Expedition in January/February 2019. The symbols represent the different regions of the Weddell Sea sampled during the expedition (circle – Antarctic Peninsula (AP); cross – FIS; triangle – LCIS; plus sign – Weddell Gyre (WG)). The general cyclonic circulation of the Weddell Gyre (dashed blue arrow) is illustrated on the central map, and the dashed black arrows indicate the input of modified water masses from Filchner-Ronne Ice shelf (FRIC) and LCIS (Gordon et al. 1993; Schröder et al. 2002; Schodlok et al. 2002). The hypothesized circulation at LCIS (Nicholls et al. 2004; Hutchinson et al. 2020) is shown by the dashed blue arrow in insert (a). The 3.125 km sea-ice concentration data shown in the central panel were taken from ftp://ftp-projects.cen.uni-hamburg.de/seaice/AMSR2/3.125km and the bathymetry data (inserts a and b) were taken from ETOPO1 (NOAA National Geophysical Data Center 2009).

Figure 2. Depth profiles (0-100 m) of (a) potential density (σ_θ), (b) potential temperature, (c) absolute salinity, and (d) photosynthetically active radiation (PAR) at all stations. The inserts in panels (a), (b) and (c) show the

978   profiles down to 1500 m, with the various water masses present at each station identified from their temperature

979   and salinity ranges (WSBW – Weddell Sea Bottom Water, WSDW – Weddell Sea Deep Water, WDW – Warm

980   Deep Water, MWDW – Modified Warm Deep Water, ISW – Ice Shelf Water, HSSW – High Salinity Shelf Water,

981   WW – Winter Water, ASW – Antarctic Surface Water). The station positions are indicated by the different

982   colours: red – Antarctic Peninsula, green – Larsen C Ice Shelf, blue –Weddell Gyre, light purple – early summer

983   Fimbul Ice Shelf, and dark purple – late summer Fimbul Ice Shelf.

984

985   **Figure 3.** Depth profiles (0-500 m) of the concentrations of (a) NH_4^+, (b) urea-N, (c) NO_2^-, (d) NO_3^-, (e) $Si(OH)_4$

986   and (f) PO_4^{3-}. For all panels, the error bars represent $\pm$ 1 SD replicate samples (n = 2-3). Where applicable, the

987   error has been propagated according to standard statistical practices.

988

989   **Figure 4.** Depth profiles (0-150 m) of (a) NO_3^- depletion, (b) $Si(OH)_4$ depletion and (c) PO_4^{3-} depletion at each

990   station. Also shown are scatterplots of (d) $Si(OH)_4$ depletion versus NO_3^- depletion at each depth over the euphotic

991   zone at all stations (grey symbols) and the theoretical euphotic zone-averaged $Si(OH)_4$ versus total N depletion

992   (coloured symbols; see text for details) and (e) PO_4^{3-} depletion versus NO_3^- depletion at each depth over the

993   euphotic zone at all stations (grey symbols) and the theoretical euphotic zone-averaged PO_4^{3-} versus total N

994   depletion (coloured symbols). The dashed line in panel (d) represents the 1:1 Si:N depletion ratio, expected for

995   iron-replete diatoms (Ragueneau et al. 2000; Hutchins and Bruland 1998; Takeda 1998; Mosseri et al. 2008),

996   while the dotted lines represent the 1:2 Si:N ratio, indicative of enhanced activity of non-siliceous phytoplankton,

997   and the 2:1 Si:N ratio, expected for iron-limited diatoms (Arrigo et al. 1999; Franck et al. 2000; Brzezinski et al.

998   2003; Green and Sambrotto 2006; Mosseri et al. 2008; Weber and Deutsch 2010; Martiny et al. 2013). The dashed

999   line in panel (e) represents the 16:1 N:P depletion ratio (the Redfield ratio), while the dotted lines represent the

1000   20:1 N:P ratio, expected for *P. antarctica*, and 14:1 N:P ratio, expected for iron-replete diatoms (Hutchins and

1001   Bruland 1998; Takeda 1998; Arrigo et al. 1999; Ragueneau et al. 2000; Mosseri et al. 2008).

1002

1003   **Figure 5.** Bar plots of (a, c, e) PON concentrations and (b, d,f) biomass C:N ratios measured at the 55% (a-b),

1004   10% (c-d) and 1% light levels (e-f). The dotted black line in panels (b), (d), and (f) indicates the Redfield C:N

1005   ratio of 6.63. The error bars represent $\pm$ 1 SD of replicate samples (n = 2-6). Where applicable, the error has been

1006   propagated according to standard statistical practices.

1007

1008   **Figure 6.** Daily rates of (a, e, i) NPP, (b, f, j) ρNO_3^-, (c, g, k) ρNH_4^+ and (d, h, l) ρurea for the 55% (a-d), 10% (e-

1009   h) and 1% light level (i-l). Where there are no bars in panels (d), (h) and (l), no data are available. The error bars

1010   represent $\pm$ 1 SD of replicate samples (n = 2).

1011

1012   **Figure 7.** Depth profiles of the NO_2^- oxidation rates measured at each station (a) between the surface and 500 m,

1013   and (b) within the euphotic zone only.

1014

1015   **Figure 8.** Euphotic zone-integrated f-ratios at each station. The hashed and white bars show the difference

1016   between the f-ratio(excluding urea) (higher value) and the f-ratio(including urea) (lower value), with the hashed bars

1017 representing the stations where urea uptake was measured and the white bars where it was estimated (see text for

1018 details).

1019

1020 **Figure 9.** The (a, d) cell counts, (b, e) relative cell abundance**,** (c) log-transformed biovolume and (f) carbon

1021 biomass of all phytoplankton groups identified from the (a-c) surface flow cytometry samples and (d-f)

1022 phytoplankton net samples. Where there are no bars in panels (d), (e), and (f), no data are available. Carbon

1023 biomass estimates in panel (f) are only available for prymnesiophyte, *P. antarctica*, and the diatom species.

1024

1025 **Figure 10.** Euphotic zone-averaged rates of (a) NPP, (b) ρNO_3^- and (c) ρNH_4^+ versus Z_{eu}, and (d) NPP versus SST

1026 at each station. The symbols in panels (b) and (c) are coloured by nutrient concentration and in panel (d), by ρNO_3^-

1027 .

1028

1029 **Figure 11.** Maps of (a) SST, (b) sea surface salinity, and (c) surface oxygen concentrations, and (d) depth profiles

1030 of oxygen concentrations in the region of LCIS at the time of sampling. SST and salinity data were acquired from

1031 the underway (~7 m inflow) ferrybox, while the oxygen concentrations were measured via the oxygen sensor on

1032 the CTD profiler, calibrated against discrete seawater samples measured for dissolved oxygen by Winkler titration

1033 (Carpenter 1965; Grasshoff et al. 1983; Hutchinson et al. 2020)(Carpenter 1965; Grasshoff, Kremling, and

1034 Ehrhard 1983)(Carpenter 1965; Grasshoff, Kremling, and Ehrhard 1983)(Carpenter 1965; Grasshoff, Kremling,

1035 and Ehrhard 1983)(Carpenter 1965; Grasshoff, Kremling, and Ehrhard 1983). The symbols in panel (d) are

1036 coloured by potential density (σ_θ), with the circles indicating the non-upwelling stations and the triangles the

1037 upwelling stations. The grey box in panel (d) indicates the average mixed layer depth (MLD) across the stations

1038 at LCIS. The bathymetry data in panels (a-c) were taken from ETOPO1 (NOAA National Geophysical Data Center

1039 2009).

1040

1041 **Figure 12.** (a) NO_3^- uptake normalised to NH_4^+ uptake versus NH_4^+ concentration and b) NO_3^- depletion versus

1042 NH_4^+ concentration. The symbols in panel (a) are coloured by NH_4^+ uptake rate and in panel (b) by PON

1043 concentration. The symbol size in panel (b) represents the light level at which the samples were incubated. In

1044 panel (b), NO_3^- depletion at LCIS corresponds with the primary y-axis and NO_3^- depletion at all other stations

1045 corresponds with the secondary y-axis.

1046

1047 **Table 1.** Euphotic zone-averaged nutrient concentrations, nutrient depletions, and nutrient depletion ratios at each

1048 station occupied in the Weddell Sea in summer 2018/2019. Values shown are averages ± 1 SD (n ≥ 2). "-" indicates

1049 no available data.

1050

1051 **Table 2.** Euphotic zone-integrated rates and averages at each station occupied in the Weddell Sea in summer

1052 2018/2019. Values shown are averages ± 1 SD (n ≥ 2). "-" indicates no available data and the values shown in

1053 italics (i.e., ρurea) were estimated rather than measured (see text for details).

1054

1055

1056

7. Author contributions

RF led the study and writing of the manuscript. SF contributed substantially to writing the manuscript, and designed the experiments with RF and TB. RF and JB carried out the experiments. JB, TB, SF, KS and SS assisted with sampling and data generations, and contributed to writing the manuscript.

9. References

Altabet, Mark A., and Roger Francois. 2001. "Nitrogen Isotope Biogeochemistry of the Antarctic Polar Frontal Zone at 170°W." *Deep-Sea Research Part II: Topical Studies in Oceanography* 48 (19–20): 4247–73. https://doi.org/10.1016/S0967-0645(01)00088-1.

Arrigo, Kevin R., and Gert L. van Dijken. 2003. "Phytoplankton Dynamics within 37 Antarctic Coastal Polynya Systems." *Journal of Geophysical Research: Oceans* 108 (8). https://doi.org/10.1029/2002jc001739.

Arrigo, Kevin R., Gert van Dijken, and Matthew Long. 2008. "Coastal Southern Ocean: A Strong Anthropogenic CO2 Sink." *Geophysical Research Letters* 35 (21): 1–6. https://doi.org/10.1029/2008GL035624.

Arrigo, Kevin R., Giacomo R. DiTullio, Robert B. Dunbar, Dale H. Robinson, Michael VanWoert, Denise L. Worthen, and Michael P. Lizotte. 2000. "Phytoplankton Taxonomic Variability in Nutrient Utilization and Primary Production in the Ross Sea." *Journal of Geophysical Research: Oceans* 105 (C4): 8827–46. https://doi.org/10.1029/1998jc000289.

Arrigo, Kevin R., Dale H. Robinson, Denise L. Worthen, Robert B. Dunbar, Giacomo R. DiTullio, Michael VanWoert, and Michael P. Lizotte. 1999. "Phytoplankton Community Structure and the Drawdown of Nutrients and CO2 in the Southern Ocean." *Science* 283 (5400): 365–67. https://doi.org/10.1126/science.283.5400.365.

1097   Assmy, Philipp, Victor Smetacek, Marina Montresor, Christine Klaas, Joachim Henjes, Volker H Strass, Jesús
1098   M Arrieta, et al. 2013. "Thick-Shelled, Grazer-Protected Diatoms Decouple Ocean Carbon and Silicon
1099   Cycles in the Iron-Limited Antarctic Circumpolar Current." *Proceedings of the National Academy of*
1100   *Sciences of the United States of America* 110 (51): 20633–38. https://doi.org/10.1073/pnas.1309345110.
1101   Baar, Hein J W De, Philip W Boyd, Kenneth H Coale, Michael R Landry, Atsushi Tsuda, Philipp Assmy,
1102   Dorothee C E Bakker, et al. 2005. "Synthesis of Iron Fertilization Experiments: From the Iron Age in the
1103   Age of Enlightenment." *JOURNAL OF GEOPHYSICAL RESEARCH* 110: 9–16.
1104   https://doi.org/10.1029/2004JC002601.
1105   Bendschneider, Kenneth, Rex J. Robinson, John H. Margeson, Jack C. Suggs, M. Rodney Midgett, Cadmium
1106   Reduction Method, R. Dussin, et al. 2020. "A New Spectrophotometric Method for the Determination of
1107   Nitrite in Sea Water." *Journal of Marine Research* 11 (3): 0–1.
1108   https://doi.org/10.1357/0022240963213673.
1109   Berges, John A., and Margaret R. Mulholland. 2008. *Enzymes and Nitrogen Cycling. Nitrogen in the Marine*
1110   *Environment*. https://doi.org/10.1016/B978-0-12-372522-6.00032-3.
1111   Böhlke, J. K., and T. B. Coplen. 1995. "Interlaboratory Comparison of Reference Materials for Nitrogenisotope-
1112   Ratio Measurements."
1113   Böhlke, J. K., S. J. Mroczkowski, and T. B. Coplen. 2003. "Oxygen Isotopes in Nitrate: New Reference
1114   Materials for 18O: 17O: 16O Measurements and Observations on Nitrate-water Equilibration." *Rapid*
1115   *Communications in Mass Spectrometry* 17 (16): 1835–46.
1116   Boyd, P. W., S. C. Doney, R. Strzepek, J. Dusenberry, K. Lindsay, and I. Fung. 2008. "Climate-Mediated
1117   Changes to Mixed-Layer Properties in the Southern Ocean: Assessing the Phytoplankton Response."
1118   *Biogeosciences* 5 (3): 847–64. https://doi.org/10.5194/bg-5-847-2008.
1119   Boyd, P. W., and M. J. Ellwood. 2010. "The Biogeochemical Cycle of Iron in the Ocean." *Nature Geoscience* 3
1120   (10): 675–82. https://doi.org/10.1038/ngeo964.
1121   Boyd, P. W., T. Jickells, C. S. Law, S. Blain, E. A. Boyle, K. O. Buesseler, K. H. Coale, et al. 2007. "Mesoscale
1122   Iron Enrichment Experiments 1993-2005: Synthesis and Future Directions." *Science* 315 (5812): 612–17.
1123   https://doi.org/10.1126/science.1131669.
1124   Boyd, Philip W. 2004. "Ironing out Algal Issues in the Southern Ocean." *Nature* 304 (5669): 396–97.
1125   Boyd, Philip W., and Scott C. Doney. 2002. "Modelling Regional Responses by Marine Pelagic Ecosystems to
1126   Global Climate Change." *Geophysical Research Letters* 29 (16): 53-1-53–54.
1127   https://doi.org/10.1029/2001gl014130.
1128   BRENNECKE, and W. 1921. "Die Ozeanographischen Arbeiten Der Deutschen Antarktischen Expedition
1129   1911-12." *Aus Dem Arciv Der Deutchen Seewarte* 39: 1–216. http://ci.nii.ac.jp/naid/10029032127/en/.
1130   Brzezinski, Mark A. 1985. "THE Si:C:N RATIO OF MARINE DIATOMS: INTERSPECIFIC VARIABILITY
1131   AND THE EFFECT OF SOME ENVIRONMENTAL VARIABLES." *Journal of Phycology*.
1132   https://doi.org/10.1111/j.0022-3646.1985.00347.x.
1133   Brzezinski, Mark A., Mary Lynn Dickson, David M. Nelson, and Raymond Sambrotto. 2003. "Ratios of Si, C
1134   and N Uptake by Microplankton in the Southern Ocean." *Deep-Sea Research Part II: Topical Studies in*
1135   *Oceanography* 50 (3–4): 619–33. https://doi.org/10.1016/S0967-0645(02)00587-8.
1136   Cape, Mattias R., Maria Vernet, Mati Kahru, and Gunnar Spreen. 2014. "Polynya Dynamics Drive Primary

1137   Production in the Larsen A and B Embayments Following Ice Shelf Collapse." *Journal of Geophysical*
1138   *Research: Oceans* 119 (1): 572–94. https://doi.org/10.1002/2013JC009441.

1139 Carpenter, JH. 1965. "The Chesapeake Bay Institute Technique for the Winkler Dissolved Oxygen Method."
1140   *Limnology and Oceanography* 10 (1): 141–43.

1141 Carvalho, Filipa, Josh Kohut, Matthew J. Oliver, and Oscar Schofield. 2017. "Defining the Ecologically
1142   Relevant Mixed-Layer Depth for Antarctica's Coastal Seas." *Geophysical Research Letters* 44 (1): 338–
1143   45. https://doi.org/10.1002/2016GL071205.

1144 Caspel, M. van, M. Schröder, O. Huhn, and H. H. Hellmer. 2015. "Precursors of Antarctic Bottom Water
1145   Formed on the Continental Shelf off Larsen Ice Shelf." *Deep-Sea Research Part I: Oceanographic*
1146   *Research Papers* 99: 1–9. https://doi.org/10.1016/j.dsr.2015.01.004.

1147 Cochlan, William P., and Deborah A. Bronk. 2003. "Effects of Ammonium on Nitrate Utilization in the Ross
1148   Sea, Antarctica: Implications for f-Ratio Estimates" 78 (3): 159–78. https://doi.org/10.1029/078ars10.

1149 Corre, P Le, and HJ Minas. 1983. "Distributions et Évolution Des Éléments Nutritifs Dans Le Secteur Indien de
1150   l'Océan Antarctique En Wn de Période Estivale." *Oceanologica Acta* 6: 365–81.

1151 Cota, G. F., W. O. Smith, D. M. Nelson, R. D. Muench, and L. I. Gordon. 1992. "Nutrient and Biogenic
1152   Particulate Distributions, Primary Productivity and Nitrogen Uptake in the Weddell-Scotia Sea Marginal
1153   Ice Zone during Winter." *Journal of Marine Research* 50 (1): 155–81.
1154   https://doi.org/10.1357/002224092784797764.

1155 Delmont, Tom O., Katherine M. Hammar, Hugh W. Ducklow, Patricia L. Yager, and Anton F. Post. 2014.
1156   "Phaeocystis Antarctica Blooms Strongly Influence Bacterial Community Structures in the Amundsen Sea
1157   Polynya." *Frontiers in Microbiology* 5 (DEC): 1–13. https://doi.org/10.3389/fmicb.2014.00646.

1158 Deppeler, Stacy L., and Andrew T. Davidson. 2017. "Southern Ocean Phytoplankton in a Changing Climate."
1159   *Frontiers in Marine Science* 4 (FEB). https://doi.org/10.3389/fmars.2017.00040.

1160 DeVries, T. 2014. "The Oceanic Anthropogenic CO_2 Sink: Storage, Air-Sea Fluxes, and Transports over the
1161   Industrial Era." *Global Biogeochemical Cycles* 28 (7): 631–47.

1162 Diamond, D. 1994. "QuikChem Method 10-114-21-1-B: Silicate by Flow Injection Analysis."

1163 Ditullio, G R, J M Grebmeier, K R Arrigo, and M P Lizotte. 2000. "Rapid and Early Export of Phaeocystis
1164   Antarctica Blooms in the Ross Sea , Antarctica" 404 (December 1996): 1996–99.

1165 Dortch, Q. 1990. "The Interaction between Ammonium and Nitrate Uptake in Phytoplankton." *Marine Ecology*
1166   *Progress Series* 61 (1): 183–201. https://doi.org/10.3354/meps061183.

1167 Dubelaar, George B.J., and R. R. Jonker. 2000. "Flow Cytometry as a Tool for the Study of Phytoplankton."
1168   *Scientia Marina* 64 (2): 135–56. https://doi.org/10.3989/scimar.2000.64n2135.

1169 Dugdale, R. C., and J. J. Goering. 1967. "Uptake of New and Regenerated Forms of Nitrogen in Primary
1170   Productivity." *Limnology and Oceanography* 12 (2): 196–206. https://doi.org/10.4319/lo.1967.12.2.0196.

1171 Dugdale, R C, and F P Wilkerson. 1986. "The Use of 15N to Measure Nitrogen Uptake in Eutrophic
1172   Experimental Considerations1 T2" 3 (July).

1173 Eicken, Hajo. 1993. "The Role of Sea Ice in Structuring Antarctic Ecosystems." In *Weddell Sea Ecology*, edited
1174   by Gotthilf Hempel, 3–13. Berlin, Heidelberg: Springer Berlin Heidelberg.

1175 El-Sayed, S. 1984. "Productivity of the Antarctic Waters — A Reappraisal." In *Marine Phytoplankton and*
1176   *Productivity. Lecture Notes on Coastal and Estuarine Studies.*, edited by Holm-Hansen O., Bolis L., and

1177   Gilles R., 8th ed., 19–34. Springer Berlin Heidelberg.

1178   El-Sayed, Sayed Z., and Satoru Taguchi. 1981. "Primary Production and Standing Crop of Phytoplankton along

1179   the Ice-Edge in the Weddell Sea." *Deep Sea Research Part A, Oceanographic Research Papers* 28 (9):

1180   1017–32. https://doi.org/10.1016/0198-0149(81)90015-7.

1181   Eppley, R. W., Peterson, B. 1979. "Particulate Organic Matter Flux and Planktonic New Production in the Deep

1182   Ocean." *Nature* 282: 677–80.

1183   Fahrbach, E., G. Rohardt, N. Scheele, M. Schroder, V. Strass, and A. Wisotzki. 1995. "Formation and Discharge

1184   of Deep and Bottom Water in the Northwestern Weddell Sea." *Journal of Marine Research* 53 (4): 515–

1185   38. https://doi.org/10.1357/0022240953213089.

1186   Fahrbach, E., G. Rohardt, M. Schröder, and V. Strass. 1994. "Transport and Structure of the Weddell Gyre."

1187   *Annales Geophysicae* 12 (9): 840–55. https://doi.org/10.1007/s00585-994-0840-7.

1188   Fawcett, S. E., and B. B. Ward. 2011. "Phytoplankton Succession and Nitrogen Utilization during the

1189   Development of an Upwelling Bloom." *Marine Ecology Progress Series* 428: 13–31.

1190   https://doi.org/10.3354/meps09070.

1191   Ferreira, Afonso, Raul R. Costa, Tiago S. Dotto, Rodrigo Kerr, Virginia M. Tavano, Ana C. Brito, Vanda

1192   Brotas, Eduardo R. Secchi, and Carlos R.B. Mendes. 2020. "Changes in Phytoplankton Communities

1193   Along the Northern Antarctic Peninsula: Causes, Impacts and Research Priorities." *Frontiers in Marine*

1194   *Science* 7 (October). https://doi.org/10.3389/fmars.2020.576254.

1195   Franck, Valerie M., Mark A. Brzezinski, Kenneth H. Coale, and David M. Nelson. 2000. "Iron and Silicic Acid

1196   Concentrations Regulate Si Uptake North and South of the Polar Frontal Zone in the Pacific Sector of the

1197   Southern Ocean." *Deep-Sea Research Part II: Topical Studies in Oceanography* 47 (15–16): 3315–38.

1198   https://doi.org/10.1016/S0967-0645(00)00070-9.

1199   Fripiat, F., D. M. Sigman, S. E. Fawcett, P. A. Rafter, M. A. Weigand, and J.-L. Tison. 2014. "New Insights into

1200   Sea Ice Nitrogen Biogeochemical Dynamics from the Nitrogen Isotopes." *Global Biogeochemical Cycles*

1201   28 (2): 115–30. https://doi.org/10.1002/2013GB004729.

1202   Frölicher, T. L., J. L. Sarmiento, D. J. Paynter, J. P. Dunne, J. P. Krasting, and M Winton. 2015. "Dominance of

1203   the Southern Ocean in Anthropogenic Carbon and Heat Uptake in CMIP5 Models." *Journal of Climate* 28

1204   (2): 862–86.

1205   Garcia, Nathan S., Julie Sexton, Tracey Riggins, Jeff Brown, Michael W. Lomas, and Adam C. Martiny. 2018.

1206   "High Variability in Cellular Stoichiometry of Carbon, Nitrogen, and Phosphorus within Classes of

1207   Marine Eukaryotic Phytoplankton under Sufficient Nutrient Conditions." *Frontiers in Microbiology* 9

1208   (MAR): 1–10. https://doi.org/10.3389/fmicb.2018.00543.

1209   Gill, A. E. 1973. "Circulation and Bottom Water Production in the Weddell Sea." *Deep-Sea Research and*

1210   *Oceanographic Abstracts* 20 (2): 111–40. https://doi.org/10.1016/0011-7471(73)90048-X.

1211   Gleitz, Markus, Michiel Rutgers Michiel, David N. Thomas, Gerhard S. Dieckmann, and Frank J. Millero. 1995.

1212   "Comparison of Summer and Winter Inorganic Carbon, Oxygen and Nutrient Concentrations in Antarctic

1213   Sea Ice Brine." *Marine Chemistry* 51 (2): 81–91. https://doi.org/10.1016/0304-4203(95)00053-T.

1214   Glibert, Patricia M., Frances P. Wilkerson, Richard C. Dugdale, John A. Raven, Christopher L. Dupont, Peter R.

1215   Leavitt, Alexander E. Parker, Joann M. Burkholder, and Todd M. Kana. 2016. "Pluses and Minuses of

1216   Ammonium and Nitrate Uptake and Assimilation by Phytoplankton and Implications for Productivity and

1217   Community Composition, with Emphasis on Nitrogen-Enriched Conditions." *Limnology and*

1218   *Oceanography* 61 (1): 165–97. https://doi.org/10.1002/lno.10203.

1219   Goeyens, L. 1991. "Ammonium Regeneration in the Scotia-Weddell Confluence Area during Spring 1988."

1220   *Marine Ecology Progress Series* 78 (3): 241–52. https://doi.org/10.3354/meps078241.

1221   Goeyens, L., P. Tréguer, M. E.M. Baumann, W. Baeyens, and F. Dehairs. 1995. "The Leading Role of

1222   Ammonium in the Nitrogen Uptake Regime of Southern Ocean Marginal Ice Zones." *Journal of Marine*

1223   *Systems* 6 (4): 345–61. https://doi.org/10.1016/0924-7963(94)00033-8.

1224   Goffart, A., G. Catalano, and J. H. Hecq. 2000. "Factors Controlling the Distribution of Diatoms and

1225   Phaeocystis in the Ross Sea." *Journal of Marine Systems* 27 (1–3): 161–75.

1226   https://doi.org/10.1016/S0924-7963(00)00065-8.

1227   Gonfiantini, R. 1984. "Stable Isotope Reference Samples for Geochemical and Hydrological Investigations."

1228   *Report of Advisory Group, Vienna.*

1229   Gordon, A. L., Huber, B. A., Hellmer, H. H., & Ffield, A. 1993. "Deep and Bottom Water of the Weddell Sea's

1230   Western Rim." *Science* 265 (5130): 95–97.

1231   Granger, Julie, and Daniel M. Sigman. 2009. "Removal of Nitrite with Sulfamic Acid for Nitrate N and O

1232   Isotope Analysis with the Denitrifier Method." *Rapid Communications in Mass Spectrometry* 23 (23):

1233   3753–62. https://doi.org/10.1002/rcm.4307.

1234   Grasshoff, K. 1976. *Methods of Seawater Analysis*. Weinheim and New York: Verlag Chemie.

1235   Grasshoff, K, K Kremling, and M Ehrhard. 1983. *Methods of Seawater Analysis*. Florida: Verlag Chemia.

1236   Green, Sara E., and Raymond N. Sambrotto. 2006. "Plankton Community Structure and Export of C, N, P and

1237   Si in the Antarctic Circumpolar Current." *Deep-Sea Research Part II: Topical Studies in Oceanography*

1238   53 (5–7): 620–43. https://doi.org/10.1016/j.dsr2.2006.01.022.

1239   Gruber, N., D. Clement, B. R. Carter, R. A. Feely, S. Van Heuven, and M. Hoppema. 2019. "The Oceanic Sink

1240   for Anthropogenic CO2 from 1994 to 2007." *Science* 363: 1193–99.

1241   Guerrero, Maria A., and Ronald D. Jones. 1996. "Photoinhibition of Marine Nitrifying Bacteria. II. Dark

1242   Recovery after Monochromatic or Polychromatic Irradiation." *Marine Ecology Progress Series* 141: 193–

1243   98. https://doi.org/10.3354/meps141193.

1244   Hansen, B, Bjornsen PK, Hansen PJ. 1994. "The Size Ratio between Planktonic Predators and Their Prey."

1245   *Limnology and Oceanography* 39 (2): 395–403.

1246   Henley, Sian F., Robyn E. Tuerena, Amber L. Annett, Anthony E. Fallick, Michael P. Meredith, Hugh J.

1247   Venables, Andrew Clarke, and Raja S. Ganeshram. 2017. "Macronutrient Supply, Uptake and Recycling

1248   in the Coastal Ocean of the West Antarctic Peninsula." *Deep-Sea Research Part II: Topical Studies in*

1249   *Oceanography* 139 (xxxx): 58–76. https://doi.org/10.1016/j.dsr2.2016.10.003.

1250   Holmes, R M, A Aminot, R Kerouel, B A Hooker, and B J Peterson. 1999. "A Simple and Precise Method for

1251   Measuring Ammonium in Marine and Freshwater Ecosystems." *Canadian Journal of Fisheries and*

1252   *Aquatic Sciences.* https://doi.org/10.1139/cjfas-56-10-1801.

1253   Hoppema, M., and L. Goeyens. 1999. "Redfield Behavior of Carbon, Nitrogen, and Phosphorus Depletions in

1254   Antarctic Surface Water." *Limnology and Oceanography* 44 (1): 220–24.

1255   https://doi.org/10.4319/lo.1999.44.1.0220.

1256   Hoppema, M, R Middag, H de Baar, E Fahrbach, E van Weerlee, and H Thomas. 2007. "Whole Season Net

1257   Community Production in the Weddell Sea." *Polar Biology* 31: 101–11.

1258   Hoppema, Mario. 2004. "Weddell Sea Is a Globally Significant Contributor to Deep-Sea Sequestration of

1259   Natural Carbon Dioxide." *Deep-Sea Research Part I: Oceanographic Research Papers* 51 (9): 1169–77.

1260   https://doi.org/10.1016/j.dsr.2004.02.011.

1261   Hoppema, Mario, Karel Bakker, Steven MAC van Heuven, Jan C van Ooijen, and Hein JW de Baar. 2015.

1262   "Distributions, Trends and Inter-Annual Variability of Nutrients along a Repeat Section through the

1263   Weddell Sea (1996-2011)." https://doi.org/10.1016/j.marchem.2015.08.007.

1264   Hoppema, Mario, Leo Goeyens, and Eberhard Fahrbach. 2000. "Intense Nutrient Removal in the Remote Area

1265   off Larsen Ice Shelf (Weddell Sea)." *Polar Biology* 23 (2): 85–94.

1266   https://doi.org/10.1007/s003000050012.

1267   Hoppema, Mario, Michel H.C. Stoll, and Hein J.W. De Baar. 2000. "Co2 in the Weddell Gyre and Antarctic

1268   Circumpolar Current: Austral Autumn and Early Winter." *Marine Chemistry* 72 (2–4): 203–20.

1269   https://doi.org/10.1016/S0304-4203(00)00082-7.

1270   Horrigan, Sarah G. 1981. "Primary Production under the Ross Ice Shelf, Antarctica." *Limnology and

1271   Oceanography* 26 (2): 378–82. https://doi.org/10.4319/lo.1981.26.2.0378.

1272   Huhn, Oliver, Hartmut H. Hellmer, Monika Rhein, Christian Rodehacke, Wolfgang Roether, Michael P.

1273   Schodlok, and Michael Schröder. 2008. "Evidence of Deep- and Bottom-Water Formation in the Western

1274   Weddell Sea." *Deep-Sea Research Part II: Topical Studies in Oceanography* 55 (8–9): 1098–1116.

1275   https://doi.org/10.1016/j.dsr2.2007.12.015.

1276   Hutchins, David A., and K. W. Bruland. 1998. "Iron-Limited Growth and Si:N Ratios in a Costal Upwelling

1277   Regime." *Nature* 393 (June): 561–64.

1278   Hutchinson, Katherine, Julie Deshayes, Jean Baptiste Sallee, Julian A. Dowdeswell, Casimir de Lavergne,

1279   Isabelle Ansorge, Hermann Luyt, Tahlia Henry, and Sarah E. Fawcett. 2020. "Water Mass Characteristics

1280   and Distribution Adjacent to Larsen C Ice Shelf, Antarctica." *Journal of Geophysical Research: Oceans*

1281   125 (4): 0–2. https://doi.org/10.1029/2019JC015855.

1282   Ito, T, M Woloszyn, and & M Mazloff. 2010. "Anthropogenic Carbon Dioxide Transport in the Southern Ocean

1283   Driven by Ekman Flow" 463 (7). https://doi.org/10.1038/nature08687.

1284   Jacobs, S. S. 1986. "The Antarctic Slope Front." *Antarct. JUS* 21 (5): 123–24.

1285   Jacobs, Stanley S. 1991. "On the Nature and Significance of the Antarctic Slope Front." *Marine Chemistry* 35

1286   (1–4): 9–24. https://doi.org/10.1016/S0304-4203(09)90005-6.

1287   Jacques, G. 1991. "Is the Concept of New Production—Regenerated Production Valid for the Southern Ocean?"

1288   *Marine Chemistry* 35 (1–4): 273–86. https://doi.org/10.1016/S0304-4203(09)90022-6.

1289   Jennings, Joe C., Louis I. Gordon, and David M. Nelson. 1984. "Nutrient Depletion Indicates High Primary

1290   Productivity in the Weddell Sea." *Nature* 309 (5963): 51–54. https://doi.org/10.1038/309051a0.

1291   Jong, Jeroen De, Véronique Schoemann, Delphine Lannuzel, Peter Croot, Hein De Baar, and Jean Louis Tison.

1292   2012. "Natural Iron Fertilization of the Atlantic Sector of the Southern Ocean by Continental Shelf

1293   Sources of the Antarctic Peninsula." *Journal of Geophysical Research: Biogeosciences* 117 (1).

1294   https://doi.org/10.1029/2011JG001679.

1295   Juel Hansen, Per, Peter Koefoed Bj, and Benni Winding Hansen. 1997. "Zooplankton Grazing and Growth:

1296   Scaling within the 2-2,000-~III Body Size Range." Vol. 42.

1297   Kana, Todd M., and Patricia M. Glibert. 1987. "Effect of Irradiances up to 2000 ME M-2 s-1 on Marine
1298   Synechococcus WH7803-I. Growth, Pigmentation, and Cell Composition." *Deep Sea Research Part A,*
1299   *Oceanographic Research Papers* 34 (4): 479–95. https://doi.org/10.1016/0198-0149(87)90001-X.

1300   Kaprelyants, A. S., and D. B. Kell. 1993. "Dormancy in Stationary-Phase Cultures of Micrococcus Luteus: Flow
1301   Cytometric Analysis of Starvation and Resuscitation." *1Applied and Environmental Microbiology* 59 (10):
1302   3187–96.

1303   Keffer, T., and G. Holloway. 1988. "Estimating Southern Ocean Eddy Flux of Heat and Salt from Satellite
1304   Altimetry." *Nature* 332 (6165): 624–26. https://doi.org/10.1038/332624a0.

1305   Keller, D.P., L. Kriest, W. Koeve, and A. Oschlies. 2016. "Southern Ocean Biological Impacts on Global Ocean
1306   Oxygen." *Geophysical Research Letters* 43: 6469–77.

1307   Kerr, Rodrigo, Mauricio M. Mata, Carlos Rafael B. Mendes, and Eduardo R. Secchi. 2018. "Northern Antarctic
1308   Peninsula: A Marine Climate Hotspot of Rapid Changes on Ecosystems and Ocean Dynamics." *Deep-Sea*
1309   *Research Part II: Topical Studies in Oceanography* 149 (March): 4–9.
1310   https://doi.org/10.1016/j.dsr2.2018.05.006.

1311   Klunder, M. B., P. Laan, H. J. W. De Baar, R. Middag, I. Neven, and J. Van Ooijen. 2014. "Dissolved Fe across
1312   the Weddell Sea and Drake Passage: Impact of DFe on Nutrient Uptake." *Biogeosciences* 11 (3): 651–69.
1313   https://doi.org/10.5194/bg-11-651-2014.

1314   Klunder, M. B., P. Laan, R. Middag, H. J.W. De Baar, and J. C. van Ooijen. 2011. "Dissolved Iron in the
1315   Southern Ocean (Atlantic Sector)." *Deep-Sea Research Part II: Topical Studies in Oceanography* 58 (25–
1316   26): 2678–94. https://doi.org/10.1016/j.dsr2.2010.10.042.

1317   Koike, I, O Holm-Hansen, and DC Biggs. 1986. "Inorganic Nitrogen Metabolism by Antarctic Phytoplankton
1318   with Special Reference to Ammonium Cycling." *Marine Ecology Progress Series* 30 (2–3): 105–16.
1319   https://doi.org/10.3354/meps030105.

1320   Lannuzel, Delphine, Véronique Schoemann, Jeroen de Jong, Lei Chou, Bruno Delille, Sylvie Becquevort, and
1321   Jean Louis Tison. 2008. "Iron Study during a Time Series in the Western Weddell Pack Ice." *Marine*
1322   *Chemistry* 108 (1–2): 85–95. https://doi.org/10.1016/j.marchem.2007.10.006.

1323   Leblanc, K, Armand L, Assmy P, Beker B, Bode A, Breton E, Cornet V, et al. 2012. "A Global Diatom
1324   Database – Abundance, Biovolume and Biomass in the World Ocean." *Earth System Science Data* 4:
1325   419–165.

1326   Llort, Joan, Marina Lévy, Jean-Baptiste Sallée, and Alessandro Tagliabue. n.d. "Onset, Intensification, and
1327   Decline of Phytoplankton Blooms in the Southern Ocean." *Journal of Marine Science* 72: 1971–84.
1328   https://doi.org/10.1093/icesjms/fsv053.

1329   Locarnini, R. A., T. Whitworth, and W. D. Nowlin. 1993. "The Importance of the Scotia Sea on the Outflow of
1330   Weddell Sea Deep Water." *Journal of Marine Research* 51 (1): 135–53.
1331   https://doi.org/10.1357/0022240933223846.

1332   Lomas, M. W., and P. M. Glibert. 1999. "Interactions between NH4/+ and NO3/- Uptake and Assimilation:
1333   Comparison of Diatoms and Dinoflagellates at Several Growth Temperatures." *Marine Biology* 133 (3):
1334   541–51. https://doi.org/10.1007/s002270050494.

1335   Malone, T. 1980. "Size-Fractionated Primary Productivity of Marine Phytoplankton." In *Environmental Science*
1336   *Research*, 301–19.

1337 Marchetti, A., and N. Cassar. 2009. "Diatom Elemental and Morphological Changes in Response to Iron
1338   Limitation: A Brief Review with Potential Paleoceanographic Applications." *Geobiology* 7 (4): 419–31.
1339   https://doi.org/10.1111/j.1472-4669.2009.00207.x.
1340 Marchetti, Adrian, and Maria T Maldonado. 2016. *The Physiology of Microalgae*. *The Physiology of*
1341   *Microalgae*. https://doi.org/10.1007/978-3-319-24945-2.
1342 Martin, John H., R. Michael Gordon, and Steve E. Fitzwater. 1991. "Iron Limitation." *Limnology and*
1343   *Oceanography* 36 (8): 1793–1802.
1344   http://doi.wiley.com/10.4319/lo.1991.36.8.1793%0Ahttp://onlinelibrary.wiley.com/store/10.4319/lo.1991.
1345   36.8.1793/asset/lno19913681793.pdf?v=1&t=j6qdk51h&s=456915f948d9c4ef90e914c1583d2396c4bfe2b
1346   6.
1347 Martínez-García, Alfredo, Daniel M Sigman, Haojia Ren, Robert F Anderson, Marietta Straub, David A Hodell,
1348   Samuel L Jaccard, Timothy I Eglinton, and Gerald H Haug. 2014. "Iron Fertilization of the Subantarctic
1349   Ocean During the Last Ice Age." www.sciencemag.org.
1350 Martiny, Adam C, Chau T A Pham, Francois W Primeau, Jasper A Vrugt, J Keith Moore, Simon A Levin, and
1351   Michael W Lomas. 2013. "Strong Latitudinal Patterns in the Elemental Ratios of Marine Plankton and
1352   Organic Matter." *Nature Geoscience*. https://doi.org/10.1038/NGEO1757.
1353 Mathot, Sylvie, Walker O. Smith, Craig A. Carlson, David L. Garrison, Marcia M. Gowing, and Chrystal L.
1354   Vickers. 2000. "Carbon Partitioning within Phaeocystis Antarctica (Prymnesiophyceae) Colonies in the
1355   Ross Sea, Antarctica." *Journal of Phycology* 36 (6): 1049–56. https://doi.org/10.1046/j.1529-
1356   8817.2000.99078.x.
1357 McIlvin, Matthew R., and Karen L. Casciotti. 2011. "Technical Updates to the Bacterial Method for Nitrate
1358   Isotopic Analyses." *Analytical Chemistry* 83 (5): 1850–56. https://doi.org/10.1021/ac1028984.
1359 Mdutyana, Mhlangabezi, Sandy J. Thomalla, Raissa Philibert, Bess B. Ward, and Sarah E. Fawcett. 2020. "The
1360   Seasonal Cycle of Nitrogen Uptake and Nitrification in the Atlantic Sector of the Southern Ocean."
1361   *Global Biogeochemical Cycles* 34 (7): 1–29. https://doi.org/10.1029/2019GB006363.
1362 Merbt, Stephanie N, David A Stahl, Emilio O Casamayor, Eugè Nia Martí, Graeme W Nicol, and James I
1363   Prosser. n.d. "Differential Photoinhibition of Bacterial and Archaeal Ammonia Oxidation."
1364   https://doi.org/10.1111/j.1574-6968.2011.02457.x.
1365 Mosby, H. 1934. "The Waters of the Atlantic Anarctic Ocean." *Science Research Norweigan Antarctic*
1366   *Expedition 1927-1928* 11: 1–311.
1367 Mosseri, Julie, Bernard Quéguiner, Leanne Armand, and Véronique Cornet-Barthaux. 2008. "Impact of Iron on
1368   Silicon Utilization by Diatoms in the Southern Ocean: A Case Study of Si/N Cycle Decoupling in a
1369   Naturally Iron-Enriched Area." *Deep-Sea Research Part II: Topical Studies in Oceanography* 55 (5–7):
1370   801–19. https://doi.org/10.1016/j.dsr2.2007.12.003.
1371 Muench, R. D., and A. L. Gordon. 1995. "Circulation and Transport of Water along the Western Weddell Sea
1372   Margin." *Journal of Geophysical Research* 100 (C9): 18503–15. https://doi.org/10.1029/95jc00965.
1373 Myung Gil, Park, Tang Sung Ryull, Kang Sung-Ho, Chung Kyung Ho, and Shim Jae Hyung. 1999.
1374   "Phytoplankton Biomass and Primary Production in the Marginal Ice Zone of the Northwestern Weddell
1375   Sea during Austral Summer." *Polar Biology* 21: 251–61.
1376 Nelson, M, O Smith, I Gordon, and A Huber. 1987. "Nutrient" 92: 7181–90.

1377   Nicholls, K. W., C. J. Pudsey, and P. Morris. 2004. "Summertime Water Masses off the Northern Larsen C Ice
1378   Shelf, Antarctica." *Geophysical Research Letters* 31 (9): 2–5. https://doi.org/10.1029/2004GL019924.
1379   Nicholls, Keith W., Svein Østerhus, Keith Makinson, Tor Gammelsrød, and Eberhard Fahrbach. 2009. "Ice-
1380   Ocean Processes over the Continental Shelf of the Southern Weddell Sea, Antarctica: A Review." *Reviews
1381   of Geophysics* 47 (3): 1–23. https://doi.org/10.1029/2007RG000250.
1382   Nissen, Cara, and Meike Vogt. 2020. "Factors Controlling the Competition between
1383   <I>Phaeocystis</I> and Diatoms in the Southern Ocean." *Biogeosciences Discussions*, no.
1384   January: 1–39. https://doi.org/10.5194/bg-2019-488.
1385   Olson, Robert J. 1981. "DIFFERENTIAL PHOTOINHIBITION OF MARINE NITRIFYING BACTERIA: A
1386   POSSIBLE MECHANISM FOR THE FORMATION OF THE PRIMARY NITRITE MAXIMUM."
1387   *Journal of Marine Research* 39 (2): 227–38.
1388   Orsi, Alejandro H., Worth D. Nowlin, and Thomas Whitworth. 1993. "On the Circulation and Stratification of
1389   the Weddell Gyre." *Deep-Sea Research Part I* 40 (1): 169–203. https://doi.org/10.1016/0967-
1390   0637(93)90060-G.
1391   Orsi, Alejandro H., Thomas Whitworth, and Worth D. Nowlin. 1995. "On the Meridional Extent and Fronts of
1392   the Antarctic Circumpolar Current." *Deep-Sea Research Part I* 42 (5): 641–73.
1393   https://doi.org/10.1016/0967-0637(95)00021-W.
1394   Parsons, T.R., Y. Maita, and C.M. Lalli. 1984. *A Manual of Chemical and Biological Methods for Seawater
1395   Analysis.*
1396   Paulsen, M. L., K. Riisgaard, T. F. Thingstad, M. S. John, and T. G. Nielsen. 2015. "Winter-Spring Transition in
1397   the Subarctic Atlantic: Microbial Response to Deep Mixing and Pre-Bloom Production." *Aquatic
1398   Microbial Ecology2* 76 (1): 49–49.
1399   Peng, X., C. A. Fuchsman, A. Jayakumar, S. Oleynik, W. Martens-Habbena, A. H. Devol, and B. B. Ward.
1400   2015. "Ammonia and Nitrite Oxidation in the Eastern Tropical North Pacific." *Global Biogeochemical
1401   Cycles2* 29: 2034–49.
1402   Peng, Xuefeng, Sarah E Fawcett, Nicolas Van Oostende, Martin J Wolf, Dario Marconi, Daniel M Sigman, and
1403   Bess B Ward. 2018. "Nitrogen Uptake and Nitrification in the Subarctic North Atlantic Ocean."
1404   https://doi.org/10.1002/lno.10784.
1405   Petrou, Katherina, Sven A. Kranz, Scarlett Trimborn, Christel S. Hassler, Sonia Blanco Ameijeiras, Olivia
1406   Sackett, Peter J. Ralph, and Andrew T. Davidson. 2016. "Southern Ocean Phytoplankton Physiology in a
1407   Changing Climate." *Journal of Plant Physiology* 203: 135–50.
1408   https://doi.org/10.1016/j.jplph.2016.05.004.
1409   Pörtner, Hans Otto, D.M. Karl, P. W. Boyd, W.W. Cheung, S E Lluch-Cota, Y. Nojiri, and Al. Et. 2014. "Ocean
1410   Systems." In *Impacts, Adaptation, and Vulnerability. Part A: Global and Sectoral Aspects. Contribution
1411   of Working Group II to the Fifth Assessment Report of the Intergovernmental Panel on Climate Change*,
1412   edited by C.B. Field and Al. Et, 411–84. Cambridge University Press.
1413   Priddle, J., I. L. Boyd, M. J. Whitehouse, E. J. Murphy, and J. P. Croxall. 1998. "Estimates of Southern Ocean
1414   Primary Production - Constraints from Predator Carbon Demand and Nutrient Drawdown." In *Journal of
1415   Marine Systems*, 17:275–88. Elsevier. https://doi.org/10.1016/S0924-7963(98)00043-8.
1416   Probyn, T. A., and S. J. Painting. 1985. "Nitrogen Uptake by Size-fractionated Phytoplankton Populations in

1417   Antarctic Surface Waters." *Limnology and Oceanography* 30 (6): 1327–32.

1418   https://doi.org/10.4319/lo.1985.30.6.1327.

1419   Qin, Wei, Shady A. Amin, Willm Martens-Habbena, Christopher B. Walker, Hidetoshi Urakawa, Allan H.

1420   Devol, Anitra E. Ingalls, James W. Moffett, E. Virginia Armbrust, and David A. Stahl. 2014. "Marine

1421   Ammonia-Oxidizing Archaeal Isolates Display Obligate Mixotrophy and Wide Ecotypic Variation."

1422   *Proceedings of the National Academy of Sciences* 111 (34): 12504–9.

1423   https://doi.org/10.1073/PNAS.1324115111.

1424   Ragueneau, O., P. Tréguer, A. Leynaert, R. F. Anderson, M. A. Brzezinski, D. J. DeMaster, R. C. Dugdale, et al.

1425   2000. "A Review of the Si Cycle in the Modern Ocean: Recent Progress and Missing Gaps in the

1426   Application of Biogenic Opal as a Paleoproductivity Proxy." *Global and Planetary Change* 26 (4): 317–

1427   65. https://doi.org/10.1016/S0921-8181(00)00052-7.

1428   Revilla, Marta, Jeffrey Alexander, and Patricia M. Glibert. 2005. "Urea Analysis in Coastal Waters: Comparison

1429   of Enzymatic and Direct Methods." *Limnology and Oceanography: Methods* 3 (7): 290–99.

1430   https://doi.org/10.4319/lom.2005.3.290.

1431   Rönner, U., F. Sörensson, and O. Holm-Hansen. 1983. "Nitrogen Assimilation by Phytoplankton in the Scotia

1432   Sea." *Polar Biology* 2 (3): 137–47. https://doi.org/10.1007/BF00448963.

1433   Rubin, SI, Takahashi T, Chipman DW, and Goddard JG. 1998. "Primary Productivity and Nutrient Utilization

1434   Ratios in the Pacific Sector of the Southern Ocean Based on Seasonal Changes in Seawater Chemistry."

1435   *Deep Sea Research Part I: Oceanographic Research Papers* 45: 1211–34.

1436   Sallée, J. B., E. Shuckburgh, N. Bruneau, A. J. Meijers, T. J. Bracegirdle, and Z. Wang. 2013. "Assessment of

1437   Southern Ocean Mixed-layer Depths in CMIP5 Models: Historical Bias and Forcing Response." *Journal*

1438   *of Geophysical Research : Oceans* 118: 1845–62.

1439   Santoro, A. E., C. M. Sakamoto, J. M. Smith, J. N. Plant, A. L. Gehman, A. Z. Worden, K. S. Johnson, C. A.

1440   Francis, and K. L. Casciotti. 2013. "Measurements of Nitrite Production in and around the Primary Nitrite

1441   Maximum in the Central California Current." *Biogeosciences* 10 (11): 7395–7410.

1442   https://doi.org/10.5194/bg-10-7395-2013.

1443   Sarmiento, J., Toggweiler, J. 1984. "A New Model for the Role of the Oceans in Determining Atmospheric P

1444   CO2." *Nature* 308: 621–24. https://doi.org/https://doi.org/10.1038/308621a0.

1445   Sarmiento, J L, N Gruber, M A Brzezinski, and J P Dunne. 2004. "High-Latitude Controls of Thermocline

1446   Nutrients and Low Latitude Biological Productivity." *Nature* 427 (6969): 56–60.

1447   https://doi.org/10.1038/nature10605.

1448   Saxberg, Bo E.H., and B. R. Kowalski. 1979. "Generalized Standard Addition Method." *Analytical Chemistry*

1449   51 (7): 1031–38. https://doi.org/10.1021/ac50043a059.

1450   Scharek, Renate, Victor Smetacek, Eberhard Fahrbach, Louis I. Gordon, Gerd Rohardt, and Stanley Moore.

1451   1994. "The Transition from Winter to Early Spring in the Eastern Weddell Sea, Antarctica: Plankton

1452   Biomass and Composition in Relation to Hydrography and Nutrients." *Deep-Sea Research Part I* 41 (8):

1453   1231–50. https://doi.org/10.1016/0967-0637(94)90042-6.

1454   Schodlok, M. P., Hellmer, H. H.,&Beckmann, A. 2002. "On the Transport, Variability and Origin of

1455   Densewatermasses Crossing the South Scotia Ridge.E." *Deep Sea Research II: Tropical Studies in*

1456   *Oceanography* 49 (21): 4807–25.

Schoemann, Véronique, Sylvie Becquevort, Jacqueline Stefels, Véronique Rousseau, and Christiane Lancelot. 2005. "Phaeocystis Blooms in the Global Ocean and Their Controlling Mechanisms: A Review." *Journal of Sea Research* 53 (1-2 SPEC. ISS.): 43–66. https://doi.org/10.1016/j.seares.2004.01.008.

Schofield, Oscar, Travis Miles, Anne Carlijn Alderkamp, Sang Hoon Lee, Christina Haskins, Emily Rogalsky, Rachel Sipler, Robert M. Sherrell, and Patricia L. Yager. 2015. "In Situ Phytoplankton Distributions in the Amundsen Sea Polynya Measured by Autonomous Gliders." *Elementa* 3: 1–17. https://doi.org/10.12952/journal.elementa.000073.

Schröder, M., H. H. Hellmer, and J. M. Absy. 2002. "On the Near-Bottom Variability in the Northwestern Weddell Sea." *Deep-Sea Research Part II: Topical Studies in Oceanography* 49 (21): 4767–90. https://doi.org/10.1016/S0967-0645(02)00158-3.

Sedwick, Peter N., Giacomo R. Di Tullio, and Denis J. Mackey. 2000. "Iron and Manganese in the Ross Sea, Seasonal Iron Limitation in Antarctic." *Journal of Geophysical Research: Oceans* 105 (C5): 11321–36. https://doi.org/10.1029/2000JC000256.

Semeneh, M., F. Dehairs, M. Elskens, M. E.M. Baumann, E. E. Kopczynska, C. Lancelot, and L. Goeyens. 1998. "Nitrogen Uptake Regime and Phytoplankton Community Structure in the Atlantic and Indian Sectors of the Southern Ocean." *Journal of Marine Systems* 17 (1–4): 159–77. https://doi.org/10.1016/S0924-7963(98)00036-0.

Sigman, D. M., K. L. Casciotti, M. Andreani, C. Barford, M. Galanter, and J. K. Böhlke. 2001. "A Bacterial Method for the Nitrogen Isotopic Analysis of Nitrate in Seawater and Freshwater." *Analytical Chemistry* 73 (17): 4145–53. https://doi.org/10.1021/ac010088e.

Sigman, Daniel M, and Edward A Boyle[2]. 2000. "Glacial/Interglacial Variations in Atmospheric Carbon Dioxide." *NATURE*. Vol. 407. www.nature.com.

Sigman, Daniel M, Mathis P Hain, and Gerald H Haug. 2010. "The Polar Ocean and Glacial Cycles in Atmospheric CO 2 Concentration." *Nature* 466. https://doi.org/10.1038/nature09149.

Smith, J M, F P Chavez, and C A Francis. 2014. "Ammonium Uptake by Phytoplankton Regulates Nitrification in the Sunlit Ocean." *PLoS ONE* 9 (9): 108173. https://doi.org/10.1371/journal.pone.0108173.

Smith, Walker 0., and David M. Nelson. 1990. "Phytoplankton Growth and New Production in the Weddell Sea Marginal Ice Zone in the Austral Spring and Autumn." *Limnology and Oceanography* 35 (4): 809–21. https://doi.org/10.4319/lo.1990.35.4.0809.

Smith, Walker O., and Vernon L. Asper. 2001. "The Influence of Phytoplankton Assemblage Composition on Biogeochemical Characteristics and Cycles in the Southern Ross Sea, Antarctica." *Deep-Sea Research Part I: Oceanographic Research Papers* 48 (1): 137–61. https://doi.org/10.1016/S0967-0637(00)00045-5.

Spiridonov, V. A., E. M. Nöthig, M. Schröder, and A. Wisotzki. 1996. "The Onset of Biological Winter in the Eastern Weddell Gyre (Antarctica) Planktonic Community." *Journal of Marine Systems* 9 (3–4): 211–30. https://doi.org/10.1016/S0924-7963(95)00049-6.

Stammerjohn, S., R. Massom, D. Rind, and D. Martinson. 2012. "Regions of Rapid Sea Ice Change: An Inter-hemispheric Seasonal Comparison." *Geophysical Research Letters* 39: L06501.

Stefels, Jacqueline, and Maria A. Van Leeuwe. 1998. "Effects of Iron and Light Stress on the Biochemical Composition of Antarctic Phaeocystis Sp. (Prymnesiophyceae). I. Intracellular DMSP Concentrations." *Journal of Phycology* 34 (3): 486–95. https://doi.org/10.1046/j.1529-8817.1998.340486.x.

1497 Strickland, John Douglas Hipwell, and Timothy Richard Parsons. 1968. "A Practical Handbook of Seawater
1498   Analysis." *Bulletin Fisheries Research Board of Canada* 167: 81–86.

1499 Strzepek, Robert F., Maria T. Maldonado, Keith A. Hunter, Russell D. Frew, and Philip W. Boyd. 2011.
1500   "Adaptive Strategies by Southern Ocean Phytoplankton to Lessen Iron Limitation: Uptake of Organically
1501   Complexed Iron and Reduced Cellular Iron Requirements." *Limnology and Oceanography* 56 (6): 1983–
1502   2002. https://doi.org/10.4319/lo.2011.56.6.1983.

1503 Sunda, W. G., and S. A. Huntsman. 1997. "Interrelated Influence of Iron, Light and Cell Size on Marine
1504   Phytoplankton Growth." *Nature* 390 (6658): 389–92. https://doi.org/10.1038/37093.

1505 Sunda, William G., and Susan A. Huntsman. 2015. "High Iron Requirement for Growth, Photosynthesis, and
1506   Low-Light Acclimation in the Coastal Cyanobacterium Synechococcus Bacillaris." *Frontiers in
1507   Microbiology2* 6: 561.

1508 Takeda, S. 1998. "Influence of Iron Availability on Nutrient Consumption Ratio." *Nature* 393 (JUNE): 774–77.

1509 Talley, Lynne D., George L. Pickard, William J. Emery, and James H. Swift. 2011. "Southern Ocean."
1510   *Descriptive Physical Oceanography*, 437–71. https://doi.org/10.1016/b978-0-7506-4552-2.10013-7.

1511 Taylor, Brad W., Christine F. Keep, Robert O. Hall, Benjamin J. Koch, Lusha M. Tronstad, Alexander S.
1512   Flecker, and Amber J. Ulseth. 2007. "Improving the Fluorometric Ammonium Method: Matrix Effects,
1513   Background Fluorescence, and Standard Additions." *Journal of the North American Benthological Society*
1514   26 (2): 167–77. https://doi.org/10.1899/0887-3593(2007)26[167:ITFAMM]2.0.CO;2.

1515 Tréguer, Paul, Chris Bowler, Brivaela Moriceau, Stephanie Dutkiewicz, Marion Gehlen, Olivier Aumont, Lucie
1516   Bittner, et al. 2017. "Influence of Diatom Diversity on the Ocean Biological Carbon Pump." *Nature
1517   Geoscience*. https://doi.org/10.1038/s41561-017-0028-x.

1518 Treguer, PJ, and Jacques G. 1992. *Review Dynamics of Nutrients and Phytoplankton, and Fluxes of Carbon,
1519   Nitrogen and Silicon in the Antarctic Ocean*. Edited by G Hempel. Springer Berlin Heidelberg.

1520 Vernet, M., W. Geibert, M. Hoppema, P. J. Brown, C. Haas, H. H. Hellmer, W. Jokat, et al. 2019. "The Weddell
1521   Gyre, Southern Ocean: Present Knowledge and Future Challenges." *Reviews of Geophysics* 57 (3): 623–
1522   708. https://doi.org/10.1029/2018RG000604.

1523 Vogt, M., C. O'Brien, J. Peloquin, V. Schoemann, E. Breton, M. Estrada, J. Gibson, et al. 2012. "Global Marine
1524   Plankton Functional Type Biomass Distributions: ≪I≫Phaeocystis≪/I≫
1525   Spp." *Earth System Science Data* 4 (1): 107–20. https://doi.org/10.5194/essd-4-107-2012.

1526 Volk, T, and M I Hoffert. 1985. "Ocean Carbon Pumps: Analysis of Relative Strengths and Efficiencies in
1527   Ocean-Driven Atmospheric CO2 Changes." In *Geophysical Monograph Series*, edited by E T Sundquist
1528   and W. S. Broecker.

1529 Ward, B. B. 1985. "Light and Substrate Concentration Relationships with Marine Ammonium Assimilation and
1530   Oxidation Rates." *Marine Chemistry* 16 (4): 301–16. https://doi.org/10.1016/0304-4203(85)90052-0.

1531 Ward, B.B. 2005. "Temporal Variability in Nitrification Rates and Related Biogeochemical Factors in Monterey
1532   Bay, California, USA." *Marine Ecology Progress Series* 292: 97–109.
1533   https://doi.org/10.3354/meps292097.

1534 Weber, Thomas S, and Curtis Deutsch. 2010. "Ocean Nutrient Ratios Governed by Plankton Biogeography."
1535   https://doi.org/10.1038/nature09403.

1536 Whitworth, Thomas, and Worth D Nowlin. 1987. "Water Masses and Currents of the Southern Ocean at the

1537   Greenwich Meridian." *JOURNAL OF GEOPHYSICAL RESEARCH*. Vol. 92.

1538   https://doi.org/10.1029/JC092iC06p06462.

1539 Yool, Andrew, Adrian P Martin, Camila Fernández, and Darren R Clark. n.d. "The Significance of Nitrification

1540   for Oceanic New Production." https://doi.org/10.1038/nature05885.

1541 Zakem, Emily J., Alia Al-Haj, Matthew J. Church, Gert L. Van Dijken, Stephanie Dutkiewicz, Sarah Q. Foster,

1542   Robinson W. Fulweiler, Matthew M. Mills, and Michael J. Follows. 2018. "Ecological Control of Nitrite

1543   in the Upper Ocean." *Nature Communications* 9 (1). https://doi.org/10.1038/s41467-018-03553-w.

1544

1545